

GDV1 induces sexual commitment of malaria parasites by antagonizing HP1-dependent gene silencing

Michael Filarsky,^{1,2} Sabine A. Fraschka,³ Igor Niederwieser,^{1,2} Nicolas M.B. Brancucci,^{1,2} Eilidh Carrington,^{1,2} Elvira Carrió,^{1,2} Suzette Moes,⁴ Paul Jenoe,⁴ Richárd Bártfai,³ Till S. Voss^{1,2,*}

¹Swiss Tropical and Public Health Institute, Basel 4051, Switzerland

²University of Basel, Basel 4003, Switzerland

³Department of Molecular Biology, Radboud University, Nijmegen 6525GA, The Netherlands

⁴Biozentrum, University of Basel, Basel 4056, Switzerland

*Corresponding author. Email: till.voss@unibas.ch

One sentence summary:

The nuclear factor GDV1 induces gametocyte differentiation by activating expression of the master transcription factor AP2-G

Malaria is caused by *Plasmodium* parasites that proliferate in the bloodstream. During each replication cycle some parasites differentiate into gametocytes, the only forms able to infect the mosquito vector and transmit malaria. Sexual commitment is triggered by activation of AP2-G, the master transcriptional regulator of gametocytogenesis. Heterochromatin protein 1 (HP1)-dependent silencing of *ap2-g* prevents sexual conversion in proliferating parasites. Here, we identified *Plasmodium falciparum* gametocyte development 1 (GDV1) as an upstream activator of sexual commitment. We found that GDV1 targeted heterochromatin and triggered HP1 eviction thus de-repressing *ap2-g*. Expression of GDV1 was responsive to environmental triggers of sexual conversion and controlled via a *gdv1* antisense RNA. Hence, GDV1 appears to act as an effector protein that induces sexual differentiation by antagonizing HP1-dependent gene silencing.

Heterochromatin protein 1 (HP1) is a conserved regulator of heterochromatin formation, heritable gene silencing and variegated gene expression (1). In *Plasmodium falciparum*, HP1-dependent clonally variant expression allows parasites to adapt rapidly to environmental challenges encountered during infection (2-4). For example, immune evasion via antigenic variation of *var*/PfEMP1 is the hallmark of *Plasmodium* survival. Other processes, such as expression of red blood cell (RBC) invasion ligands or nutrient transporters, are similarly regulated in this parasite (4). Most clonally variant genes cluster in subtelomeric domains but some also occur in chromosome-internal heterochromatic regions. In addition, HP1 forms microdomains at some euchromatic genes (2). One of these encodes the transcription factor AP2-G that is required for sexual conversion and differentiation (2, 5-7). HP1-dependent regulation of *ap2-g* controls the rate at which parasites commit to sexual differentiation (7).

To explore the mechanisms regulating HP1 occupancy in *P. falciparum* we identified HP1-interacting proteins by liquid chromatography-tandem mass spectrometry (LC-MS/MS) analysis

of native HP1 complexes that were purified by co-immunoprecipitation (co-IP) from parasites expressing GFP-tagged HP1 (7) (Fig. 1A and Table S3). Interestingly, we consistently observed GDV1 among the potential HP1 interaction partners (Table S1). GDV1 is a nuclear protein implicated in sexual commitment and early gametocytogenesis but its exact function remains unknown (8). We therefore created a parasite line for the conditional expression of fluorescently labelled ectopic GDV1 (GDV1-GFP-DD) (Fig. 1B). Proteins tagged with the immunophilin protein-folding chaperone FKBP destabilisation domain (DD) are proteolytically degraded unless cells are cultured in presence of Shield-1, a small molecule ligand stabiliser (9, 10). Thus, GDV1-GFP-DD is barely detectable in parasites cultured in absence of Shield-1 (3D7/GDV1-GFP-DD^{OFF}), but its expression is markedly induced in parasites grown in presence of Shield-1 (3D7/GDV1-GFP-DD^{ON}) (Fig. 1, B and C). In agreement with the co-IP results GDV1-GFP-DD co-localizes with HP1 at the nuclear periphery (Fig. 1C and Fig. S1). Furthermore, we found that recombinant HP1 and GDV1 formed a complex (Fig. S1) and that HP1 co-purified with GDV1-GFP-DD in reverse co-IPs (Fig. 1D, Tables S2 and S4). The chromodomain-helicase-DNA-binding protein 1 (CHD1) and a protein of unknown function (PF3D7_1451200) also consistently co-purified with both HP1 and GDV1-GFP-DD (Tables S1 and S2). Given that CHD1 plays important roles in cell fate decision and heterochromatin remodelling in other organisms (11, 12) and that GDV1 is implicated in gametocytogenesis (8) it appears that this putative regulatory complex may function in activating sexual commitment.

Malaria parasites proliferate by iterative rounds of intra-erythrocytic replication through schizogony, merozoite release and RBC re-invasion. The decision to enter gametocytogenesis is made in the cell cycle prior to sexual differentiation; sexually committed schizonts release merozoites that invade RBCs and differentiate all into either female or male gametocytes (13, 14) (Fig. 2A). To test if GDV1 triggers sexual commitment, 3D7/GDV1-GFP-DD^{OFF} parasites were

split and cultured in the absence or presence of Shield-1. After re-invasion, stage I gametocytes were quantified by immuno-fluorescence assays (IFA) using antibodies against the gametocyte marker Pfs16 (15). Strikingly, the 3D7/GDV1-GFP-DD^{ON} population displayed a sexual conversion rate of 57.2% (+/- 10.0 SD) compared to 11.0% (+/- 2.4 SD) in 3D7/GDV1-GFP-DD^{OFF} parasites, and these gametocytes differentiated normally into both male and female gametocytes and showed a typical female-biased sex ratio (Fig. 2B and Fig. S2). Moreover, Shield-1 titration revealed a positive correlation between ectopic GDV1-GFP-DD expression levels and sexual conversion rates (Fig. 2C). To test if endogenous GDV1 levels similarly correlate with gametocyte conversion we used CRISPR/Cas9-based gene editing to append a triple hemagglutinin (HA) tag to the N-terminus of GDV1 (3D7/3xHA-GDV1) (Fig. S3). Endogenous 3xHA-GDV1 co-localised with HP1 as expected (Fig. 2D and Fig. S3) but was only expressed in some parasites. We next quantified 3xHA-GDV1 expression under conditions that either suppress or favour sexual conversion. To this end, we made use of the recent discovery of choline as an inhibitor of sexual commitment (16). 3D7/3xHA-GDV1 parasites cultured in the presence or absence of 2 mM choline displayed sexual commitment rates of 1.8% (+/- 0.3 SD) or 30.9% (+/- 3.8 SD), respectively (Fig. 2E). Strikingly, parasites cultured in the absence of choline showed markedly increased 3xHA-GDV1 expression levels (Fig. 2F). This was accounted for by a higher proportion of 3xHA-GDV1-positive cells (48.6% (+/- 3.4 SD) in absence compared to 16.4% (+/- 1.8 SD) in presence of choline) (Fig. 2F) and comparatively higher 3xHA-GDV1 expression levels in individual 3xHA-GDV1-positive parasites (Fig. S3). Together, these results show that GDV1 activates sexual conversion in a dose-dependent manner and that endogenous GDV1 expression can be induced by environmental signals triggering sexual commitment. We next performed comparative transcriptome analyses using two-colour microarrays. 3D7/GDV1-GFP-DD^{OFF} ring stage parasites were split, cultured separately in absence or presence

of Shield-1 and total RNA was harvested at seven paired time points spanning the remaining 24 hours of generation 1 (24-32 hours post-invasion (hpi); 32-40 hpi, 40-48 hpi) and the first 40 hours after re-invasion in generation 2 (8-16 hpi, 16-24 hpi, 24-32 hpi, 32-40 hpi) (Fig. 2A). As expected, GDV1-GFP-DD expression triggered a transcriptional response characteristic of sexual commitment and early differentiation. This was evident from the induction of *ap2-g* in generation 1, followed by activation of early gametocyte markers (5, 7, 8, 17) after re-invasion (Fig. 2G, Fig. S4 and Table S5). In F12 parasites, a 3D7-derived gametocyte-deficient clone carrying a loss-of-function mutation in *ap2-g* (5, 18), GDV1-GFP-DD expression still activated *ap2-g* but failed to launch a sexual differentiation response (Fig. 2H and Table S6). Next to *ap2-g* only eight other genes were significantly induced in F12/GDV1-GFP-DD^{ON} parasites, all of which are marked by HP1. This set included *dblmsp2*, which was also induced in 3D7/GDV1-GFP-DD^{ON} parasites (Fig. 2, G and H). Given that DBLMSP2 is a merozoite surface antigen expressed only in a small subpopulation of schizonts (19, 20) the GDV1-dependent activation of the *dblmsp2* locus suggests it may be expressed specifically in sexually committed schizonts. In summary, these findings show that GDV1 is an upstream activator of sexual commitment and likely triggers this process by antagonising HP1-dependent silencing of *ap2-g*.

To test if GDV1 associates with heterochromatin *in vivo* we conducted comparative ChIP-seq experiments. 3D7/GDV1-GFP-DD^{OFF} parasites were split at 28-34 hpi, cultured in parallel in the absence or presence of Shield-1 and paired chromatin samples were harvested two (30-36 hpi), six (34-40 hpi) and ten (38-44 hpi) hours after Shield-1 addition. We found that (1) GDV1-GFP-DD associates specifically with heterochromatin throughout the genome (Fig. 3A, Fig. S5, Table S7); (2) GDV1-GFP-DD occupancy was markedly higher in 3D7/GDV1-GFP-DD^{ON} compared to 3D7/GDV1-GFP-DD^{OFF} parasites (Fig. S5, Table S7); and (3) GDV1-GFP-DD occupancy is highly correlated with that of HP1 (Fig. 3B). Moreover, GDV1-GFP-DD occupancy peaked six

hours post-induction and decreased substantially thereafter (Fig. 3A, Fig. S5, Table S7). This drop in GDV1-GFP-DD signal coincided with a reduced HP1 occupancy over heterochromatic genes in 3D7/GDV1-GFP-DD^{ON} compared to 3D7/GDV1-GFP-DD^{OFF} parasites (Fig. 3, A and C, Table S7). While the vast majority of heterochromatic loci, in particular those displaying high HP1 occupancy such as *var* genes, displayed only slightly decreased HP1 levels, some genes exhibited as much as 40% reduced HP1 occupancy (Fig. 3C and Table S7). This group of genes includes *ap2-g* and most known HP1-associated early gametocyte markers including *geco* (21), *pfgexp17* (22) and *pfg14_748* (8, 17) (Fig. 3, C and D, Table S7). These data are consistent with the microarray results, where GDV1-GFP-DD expression activated *ap2-g* and early gametocyte genes but had no effect on the expression of the bulk of heterochromatic loci including *var* genes (Fig. 2, G and H). Of note, given the 50-60% sexual conversion rate observed for 3D7/GDV1-GFP-DD^{ON} parasites (see above), a 30-40% reduction in HP1 occupancy indicates that HP1 may be depleted at these loci specifically in sexually committed parasites but single cell approaches are required to confirm this hypothesis. Overall, we suggest that GDV1 destabilises heterochromatin and thus allows specific transcription factors to activate expression of *ap2-g* and other gametocyte-specific heterochromatic genes, and this may play an important role in the positive auto-regulatory feedback loop proposed to reinforce AP2-G expression in committed parasites (5, 6, 23). How GDV1 achieves specificity in unlocking specific HP1-associated genes despite binding heterochromatin genome-wide is a challenging question to be addressed in the future.

Since GDV1 activates sexual commitment, the question arises of how parasites limit GDV1 expression to prevent sexual conversion in asexual schizonts. A recent study identified a multi-exon long non-coding *gdv1* antisense RNA (asRNA) that initiates downstream of the *gdv1* locus and overlaps with the ATG start codon of *gdv1* (24), which is a hallmark feature of regulatory

asRNAs (25). To investigate if the *gdv1* asRNA participates in regulating sexual commitment we created a *gdv1* asRNA loss-of-function mutant in F12 parasites (F12/*gdv1*-asKO) (Fig. 4A and Fig. S6). Strand-specific RNA-seq analysis identified a small set of genes that were consistently differentially expressed between F12/*gdv1*-asKO and F12 wild-type parasites (17 up- and 23 down-regulated genes) (Fig. 4B, Table S8). Strikingly, and similar to F12 parasites expressing ectopic GDV1-GFP-DD (Fig. 2H), *ap2-g*, *dblmsp2* and two early gametocyte genes (*pfg14_748*, PF3D7_1477400) (8, 17) were markedly induced in F12/*gdv1*-asKO parasites, and all except one up-regulated gene are HP1-associated genes (Fig. 4B, Fig. S6, Table S8). *gdv1* sense transcripts were slightly increased in the F12/*gdv1*-asKO population, while *gdv1* antisense transcripts were undetectable as expected (Fig. 4, B and C, Fig. S6, Table S8). These results indicated that the *gdv1* asRNA acts as a negative regulator of GDV1 expression. To confirm this hypothesis, we tagged endogenous GDV1 in these parasites (F12/3xHA-GDV1/*gdv1*-asKO) and observed that indeed almost all parasites expressed 3xHA-GDV1 (96.7% +/- 2.5 SD) (Fig. S7). Lastly, we show that deletion of the *gdv1* asRNA locus in a conditional AP2-G mutant resulted in a markedly increased production of gametocytes (Fig. S8 and Supplementary text). Together, these findings demonstrate a central role for the *gdv1*-asRNA in regulating GDV1-dependent activation of sexual commitment. We anticipate this mechanism likely involves inhibiting GDV1 expression by interference with *gdv1* mRNA transcription, stability or translation, similar to asRNA-mediated gene regulation in other organisms (26).

We identified GDV1-mediated heterochromatin destabilisation as an epigenetic control strategy regulating sexual cell fate decision in *P. falciparum*. Our discovery of the *gdv1*-asRNA as a negative regulator of sexual commitment is reminiscent of lncRNA-mediated control of gametogenesis in yeasts (27, 28). In *S. cerevisiae*, nutritional stress triggers gametogenesis by activating the transcriptional regulator Inducer of Meiosis 1 (IME1) (28). A lncRNA in the *ime1*

promoter and antisense transcription of *ime4* are key factors in preventing IME1 expression under non-inducing conditions (29, 30). These parallels raise the exciting possibility that evolutionary divergent unicellular eukaryotes may employ a conceptually similar regulatory logic to control entry into the sexual phases of their life cycles. Interestingly, all *Plasmodium* species infecting humans possess a GDV1 ortholog suggesting the GDV1-based regulation of sexual commitment is conserved in all human-infective malaria parasites. In conclusion, our study contributes to understanding the molecular pathway underlying the formation of malaria transmission stages and provides opportunities for the development of intervention strategies targeting transmission of human malaria.

References and Notes:

1. S. H. Kwon, J. L. Workman, The heterochromatin protein 1 (HP1) family: put away a bias toward HP1. *Mol. Cells* **26**, 217-227 (2008).
2. C. Flueck *et al.*, Plasmodium falciparum heterochromatin protein 1 marks genomic loci linked to phenotypic variation of exported virulence factors. *PLoS. Pathog.* **5**, e1000569- (2009).
3. N. Rovira-Graells *et al.*, Transcriptional variation in the malaria parasite Plasmodium falciparum. *Genome Res* **22**, 925-938 (2012).
4. T. S. Voss, Z. Bozdech, R. Bartfai, Epigenetic memory takes center stage in the survival strategy of malaria parasites. *Curr. Opin. Microbiol.* **20**, 88-95 (2014).
5. B. F. Kafsack *et al.*, A transcriptional switch underlies commitment to sexual development in malaria parasites. *Nature* **507**, 248-252 (2014).
6. A. Sinha *et al.*, A cascade of DNA-binding proteins for sexual commitment and development in Plasmodium. *Nature* **507**, 253-257 (2014).

7. N. M. Brancucci *et al.*, Heterochromatin protein 1 secures survival and transmission of malaria parasites. *Cell Host. Microbe* **16**, 165-176 (2014).
8. S. Eksi *et al.*, Plasmodium falciparum gametocyte development 1 (Pfgdv1) and gametocytogenesis early gene identification and commitment to sexual development. *PLoS. Pathog.* **8**, e1002964- (2012).
9. L. A. Banaszynski *et al.*, A rapid, reversible, and tunable method to regulate protein function in living cells using synthetic small molecules. *Cell* **126**, 995-1004 (2006).
10. C. M. Armstrong, D. E. Goldberg, An FKBP destabilization domain modulates protein levels in Plasmodium falciparum. *Nat. Methods* **4**, 1007-1009 (2007).
11. A. Gaspar-Maia *et al.*, Chd1 regulates open chromatin and pluripotency of embryonic stem cells. *Nature* **460**, 863-868 (2009).
12. L. Bugga, I. E. McDaniel, L. Engie, J. A. Armstrong, The Drosophila melanogaster CHD1 chromatin remodeling factor modulates global chromosome structure and counteracts HP1a and H3K9me2. *PLoS. ONE.* **8**, e59496- (2013).
13. M. C. Bruce, P. Alano, S. Duthie, R. Carter, Commitment of the malaria parasite Plasmodium falciparum to sexual and asexual development. *Parasitology* **100 Pt 2**, 191-200 (1990).
14. F. Silvestrini, P. Alano, J. L. Williams, Commitment to the production of male and female gametocytes in the human malaria parasite Plasmodium falciparum. *Parasitology* **121 Pt 5**, 465-471 (2000).
15. M. C. Bruce *et al.*, Cellular location and temporal expression of the Plasmodium falciparum sexual stage antigen Pfs16. *Mol. Biochem. Parasitol.* **65**, 11-22 (1994).
16. N. M. B. Brancucci *et al.*, Lysophosphatidylcholine Regulates Sexual Stage Differentiation in the Human Malaria Parasite Plasmodium falciparum. *Cell* **171**, (2017).

17. S. Eksi *et al.*, Identification of a subtelomeric gene family expressed during the asexual-sexual stage transition in *Plasmodium falciparum*. *Mol. Biochem. Parasitol.* **143**, 90-99 (2005).
18. P. Alano *et al.*, *Plasmodium falciparum*: parasites defective in early stages of gametocytogenesis. *Exp. Parasitol.* **81**, 227-235 (1995).
19. J. A. Pearce *et al.*, Characterisation of two novel proteins from the asexual stage of *Plasmodium falciparum*, H101 and H103. *Mol. Biochem. Parasitol.* **139**, 141-151 (2005).
20. A. Amambua-Ngwa *et al.*, Population genomic scan for candidate signatures of balancing selection to guide antigen characterization in malaria parasites. *PLoS. Genet.* **8**, e1002992- (2012).
21. B. J. Morahan *et al.*, Functional analysis of the exported type IV HSP40 protein PfGECO in *Plasmodium falciparum* gametocytes. *Eukaryot. Cell* **10**, 1492-1503 (2011).
22. F. Silvestrini *et al.*, Protein export marks the early phase of gametocytogenesis of the human malaria parasite *Plasmodium falciparum*. *Mol Cell Proteomics* **9**, 1437-1448 (2010).
23. A. Poran *et al.*, Single-cell RNA sequencing reveals a signature of sexual commitment in malaria parasites. *Nature* **551**, 95-99 (2017).
24. K. M. Broadbent *et al.*, Strand-specific RNA sequencing in *Plasmodium falciparum* malaria identifies developmentally regulated long non-coding RNA and circular RNA. *BMC. Genomics* **16**, 454- (2015).
25. F. Huber *et al.*, Protein Abundance Control by Non-coding Antisense Transcription. *Cell Rep.* **15**, 2625-2636 (2016).
26. V. Pelechano, L. M. Steinmetz, Gene regulation by antisense transcription. *Nat. Rev. Genet.* **14**, 880-893 (2013).

27. E. Hiriart, A. Verdel, Long noncoding RNA-based chromatin control of germ cell differentiation: a yeast perspective. *Chromosome Res.* **21**, 653-663 (2013).
28. F. J. van Werven, A. Amon, Regulation of entry into gametogenesis. *Philos. Trans. R. Soc. Lond B Biol. Sci.* **366**, 3521-3531 (2011).
29. B. Gelfand *et al.*, Regulated antisense transcription controls expression of cell-type-specific genes in yeast. *Mol. Cell Biol.* **31**, 1701-1709 (2011).
30. F. J. van Werven *et al.*, Transcription of two long noncoding RNAs mediates mating-type control of gametogenesis in budding yeast. *Cell* **150**, 1170-1181 (2012).
31. R. Edgar, M. Domrachev, A. E. Lash, Gene Expression Omnibus: NCBI gene expression and hybridization array data repository. *Nucleic Acids Res.* **30**, 207-210 (2002).
32. P. Alano, S. Premawansa, M. C. Bruce, R. Carter, A stage specific gene expressed at the onset of gametocytogenesis in *Plasmodium falciparum*. *Mol. Biochem. Parasitol.* **46**, 81-88 (1991).
33. W. Trager, J. B. Jensen, Cultivation of malarial parasites. *Nature* **273**, 621-622 (1978).
34. C. Lambros, J. P. Vanderberg, Synchronization of *Plasmodium falciparum* erythrocytic stages in culture. *J. Parasitol.* **65**, 418-420 (1979).
35. K. Witmer *et al.*, Analysis of subtelomeric virulence gene families in *Plasmodium falciparum* by comparative transcriptional profiling. *Mol. Microbiol.* **84**, 243-259 (2012).
36. T. S. Voss *et al.*, A var gene promoter controls allelic exclusion of virulence genes in *Plasmodium falciparum* malaria. *Nature* **439**, 1004-1008 (2006).
37. M. Ghorbal *et al.*, Genome editing in the human malaria parasite *Plasmodium falciparum* using the CRISPR-Cas9 system. *Nat. Biotechnol.* **32**, 819-821 (2014).
38. T. G. Montague *et al.*, CHOPCHOP: a CRISPR/Cas9 and TALEN web tool for genome editing. *Nucleic Acids Res.* **42**, W401-W407 (2014).

39. K. Labun *et al.*, CHOPCHOP v2: a web tool for the next generation of CRISPR genome engineering. *Nucleic Acids Res.* **44**, W272-W276 (2016).
40. J. A. Thomas *et al.*, Development and Application of a Simple Plaque Assay for the Human Malaria Parasite *Plasmodium falciparum*. *PLoS. ONE.* **11**, e0157873- (2016).
41. T. S. Voss *et al.*, Identification of nuclear proteins that interact differentially with *Plasmodium falciparum* var gene promoters. *Mol Microbiol* **48**, 1593-1607 (2003).
42. J. Schindelin *et al.*, Fiji: an open-source platform for biological-image analysis. *Nat. Methods* **9**, 676-682 (2012).
43. C. A. Daubenberger *et al.*, The N'-terminal domain of glyceraldehyde-3-phosphate dehydrogenase of the apicomplexan *Plasmodium falciparum* mediates GTPase Rab2-dependent recruitment to membranes. *Biol. Chem.* **384**, 1227-1237 (2003).
44. M. P. Malakhov *et al.*, SUMO fusions and SUMO-specific protease for efficient expression and purification of proteins. *J. Struct. Funct. Genomics* **5**, 75-86 (2004).
45. C. Flueck *et al.*, A major role for the *Plasmodium falciparum* ApiAP2 protein PfSIP2 in chromosome end biology. *PLoS. Pathog.* **6**, e1000784- (2010).
46. F. W. Studier, Protein production by auto-induction in high density shaking cultures. *Protein Expr. Purif.* **41**, 207-234 (2005).
47. T. Ponnudurai, A. H. Lensen, J. F. Meis, J. H. Meuwissen, Synchronization of *Plasmodium falciparum* gametocytes using an automated suspension culture system. *Parasitology* **93** (Pt 2), 263-274 (1986).
48. R. Carter, P. M. Graves, "Gametocytes" in *Malaria: Principles and Practice of Malariology*, W. H. Wernsdorfer, I. McGregor, Eds. (Churchill Livingstone, Edinburgh, 1988), vol. 1, pp. 253-305.

49. W. A. Hoeijmakers, R. Bartfai, K. J. Francoijs, H. G. Stunnenberg, Linear amplification for deep sequencing. *Nat Protoc* **6**, 1026-1036 (2011).
50. P. R. Kensche *et al.*, The nucleosome landscape of *Plasmodium falciparum* reveals chromatin architecture and dynamics of regulatory sequences. *Nucleic Acids Res.* **44**, 2110-2124 (2016).
51. Z. Bozdech *et al.*, The transcriptome of the intraerythrocytic developmental cycle of *Plasmodium falciparum*. *PLoS. Biol.* **1**, E5- (2003).
52. H. J. Painter, L. M. Altenhofen, B. F. Kafsack, M. Llinas, Whole-genome analysis of *Plasmodium* spp. Utilizing a new agilent technologies DNA microarray platform. *Methods Mol. Biol.* **923**, 213-219 (2013).
53. V. G. Tusher, R. Tibshirani, G. Chu, Significance analysis of microarrays applied to the ionizing radiation response. *Proc. Natl. Acad. Sci. U. S. A* **98**, 5116-5121 (2001).
54. A. J. Saldanha, Java Treeview--extensible visualization of microarray data. *Bioinformatics.* **20**, 3246-3248 (2004).
55. W. A. Hoeijmakers, R. Bartfai, H. G. Stunnenberg, Transcriptome analysis using RNA-Seq. *Methods Mol. Biol.* **923**, 221-239 (2013).
56. P. Prommana *et al.*, Inducible knockdown of *Plasmodium* gene expression using the glmS ribozyme. *PLoS. ONE.* **8**, e73783- (2013).
57. P. Y. Watson, M. J. Fedor, The glmS riboswitch integrates signals from activating and inhibitory metabolites in vivo. *Nat. Struct. Mol. Biol.* **18**, 359-363 (2011).
58. W. C. Winkler *et al.*, Control of gene expression by a natural metabolite-responsive ribozyme. *Nature* **428**, 281-286 (2004).

Acknowledgements. We are grateful to M. van de Vegte-Bolmer and R. Sauerwein for determining gametocyte sex ratios and providing α -Pfs16 antibodies, to D. Richard for providing the pL6-3HA_glmS-246 plasmid and to T. Haefliger for technical assistance. This work was supported by the Swiss National Science Foundation (grant numbers 31003A_143916, 31003A_163258, BSCGIO_157729), the Foundation Pasteur Suisse and the Netherlands Organization for Scientific Research (NWO-Vidi 864.11.007). All data and code to understand and assess the conclusions of this research are available in the main text, supplementary materials and via the following repository: Gene Expression Omnibus (www.ncbi.nlm.nih.gov/geo) (31) accession GSE95549 (microarray data) and GSE94901 (ChIP-seq and RNA-seq data). M.F. designed and performed experiments, analysed data, prepared illustrations and wrote the paper. S.A.F. performed and analysed ChIP-Seq and RNA-seq experiments. I.N. designed and cloned CRISPR/Cas9 mother plasmids and performed experiments involving recombinant proteins. N.M.B.B. performed experiments related to the 3D7/3xHA-GDV1 and F12/3xHA-GDV1/*gdl1*-asKO parasites. E. Carrington performed and analysed RT-qPCR experiments. E. Carrió performed experiments involving 3D7/AP2-G-GFP-DDglmS parasites. S.M. performed LC-MS/MS experiments. P.J. provided conceptual advice. P.J., R.B and T.S.V. provided resources. R.B. designed, supervised and analysed experiments. T.S.V. conceived of the study and designed, supervised, and analysed experiments and wrote the paper. All authors contributed to editing of the manuscript.

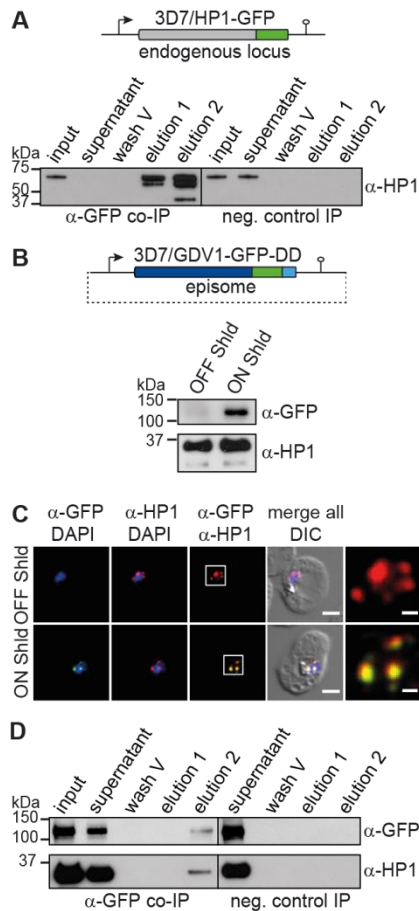


Fig. 1. GDV1 interacts with HP1. (A) Endogenous *hpl* locus in 3D7/HP1-GFP parasites and α -HP1 Western blots of the α -HP1-GFP co-IP and negative control samples. Results are representative of three biological replicates. (B) *gdv1-gfp-dd* expression plasmid and α -GFP Western blots of 3D7/GDV1-GFP-DD^{OFF} and 3D7/GDV1-GFP-DD^{ON} parasites. α -HP1 antibodies served as loading control. (C) GDV1-GFP-DD/HP1 co-localisation IFAs in 3D7/GDV1-GFP-DD^{OFF} and 3D7/GDV1-GFP-DD^{ON} trophozoites (24-32 hpi). DIC, differential interference contrast. Scale bar, 2.5 μ m (0.5 μ m for the magnified views in the rightmost images). Results are representative of three biological replicates. (D) α -GFP and α -HP1 Western blots of the α -GDV1-GFP-DD co-IP and negative control samples. Results are representative of three biological replicates.

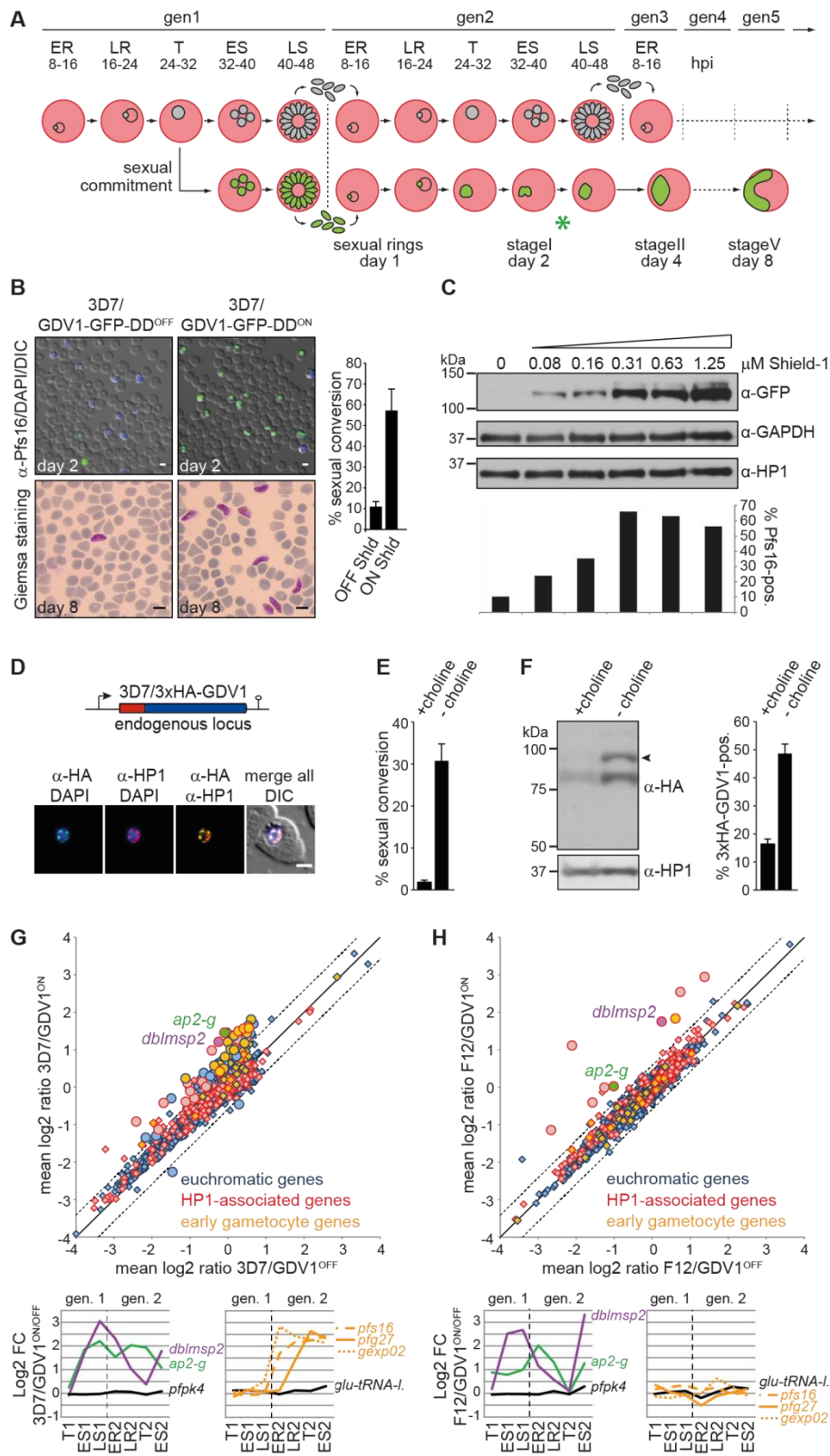


Fig. 2. GDV1 induces sexual commitment and differentiation. (A) Schematic illustrating the iterative cycles of schizogony and RBC re-invasion (top) or sexual commitment, RBC re-invasion and gametocyte differentiation (bottom). ER/LR, early/late ring stages; T, trophozoites; ES/LS, early/late schizonts; gen, generation; hpi, hours post-invasion; asterisk, time point of α -Pfs16 IFAs. (B) Top panel: α -Pfs16 IFAs identifying stage I gametocytes. Quantification of Pfs16-positive parasites is shown at the right (results are the mean of three biological replicates (200 infected RBCs counted per sample); error bars indicate SD). Bottom panel: Giemsa-stained blood smears showing stage V gametocytes. Scale bars, 5 μ m. (C) Western blot showing GDV1-GFP-DD expression in presence of increasing Shield-1 concentrations. α -GAPDH and α -HP1 antibodies served as loading controls. Percentages of Pfs16-positive parasites are shown at the bottom (400 infected RBCs counted per sample). (D) Endogenous *gdv1* locus in 3D7/3xHA-GDV1 parasites and 3xHA-GDV1/HP1 co-localisation IFAs in trophozoites (24-32 hpi). Scale bar, 2.5 μ m. (E) Sexual conversion rates in 3D7/3xHA-GDV1 parasites cultured in presence or absence of choline (results are the mean of three biological replicates (>190 infected RBCs counted per sample); error bars indicate SD). (F) Left panel: Western blot showing 3xHA-GDV1 expression levels in 3D7/3xHA-GDV1 parasites cultured in presence or absence of choline. α -HP1 antibodies served as loading control. Right panel: Percentages of 3xHA-GDV1-positive parasites in presence or absence of choline (results are the mean of three biological replicates (>100 infected RBCs counted per sample); error bars indicate SD). (G,H) Comparison of mean expression levels of all genes in 3D7/GDV1-GFP-DD^{ON} versus 3D7/GDV1-GFP-DD^{OFF} (G) and F12/GDV1-GFP-DD^{ON} versus F12/GDV1-GFP-DD^{OFF} parasites (H). Significantly de-regulated genes are indicated by circles (mean fold change cut-off >1.5; q-value (fdr) cut-off <0.15). Known early gametocyte markers (7, 8, 17) are labelled orange. Line graphs show fold changes

in expression across seven consecutive TPs. *pfs16/pfg27/gexp02*, early gametocyte markers (15, 22, 32); *pk4* (PF3D7_0628200)/*glu-tRNA-l*. (PF3D7_1331700), control genes (7).

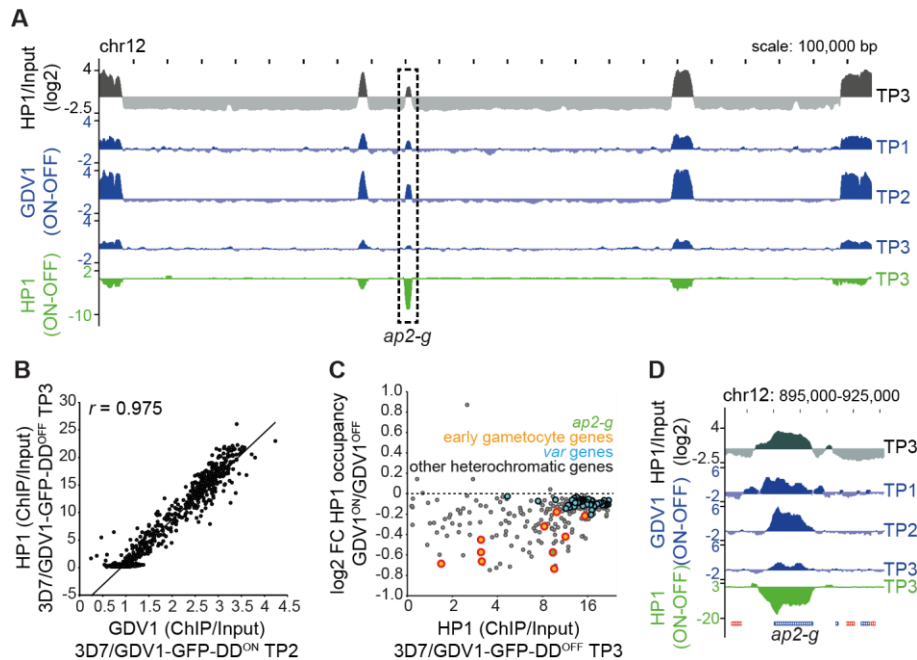


Fig. 3. GDV1 associates with heterochromatin throughout the genome and triggers HP1 removal at *ap2-g*. (A) HP1 over input ratio track from 3D7/GDV1-GFP-DD^{OFF} schizonts (38-44 hpi, TP3) (grey). ChIP-seq subtraction tracks display relative enrichment of GDV1-GFP-DD in 3D7/GDV1-GFP-DD^{ON} schizonts two (30-36 hpi, TP1), six (34-40 hpi, TP2) and ten (38-44 hpi, TP3) hours after Shield-1 addition (blue), and relative depletion of HP1 in 3D7/GDV1-GFP-DD^{ON} parasites at TP3 (green). (B) Correlation between GDV1-DD-GFP enrichment in 3D7/GDV1-GFP-DD^{ON} (34-40 hpi, TP2) and HP1 enrichment in 3D7/GDV1-GFP-DD^{OFF} schizonts at each coding region. r , Pearson correlation coefficient. (C) Fold change in HP1 enrichment upon GDV1-GFP-DD overexpression in relation to HP1 enrichment in 3D7/GDV1-GFP-DD^{OFF} schizonts for each heterochromatic gene. (D) Zoom-in view of the enrichment/subtraction tracks at the *ap2-g* locus.

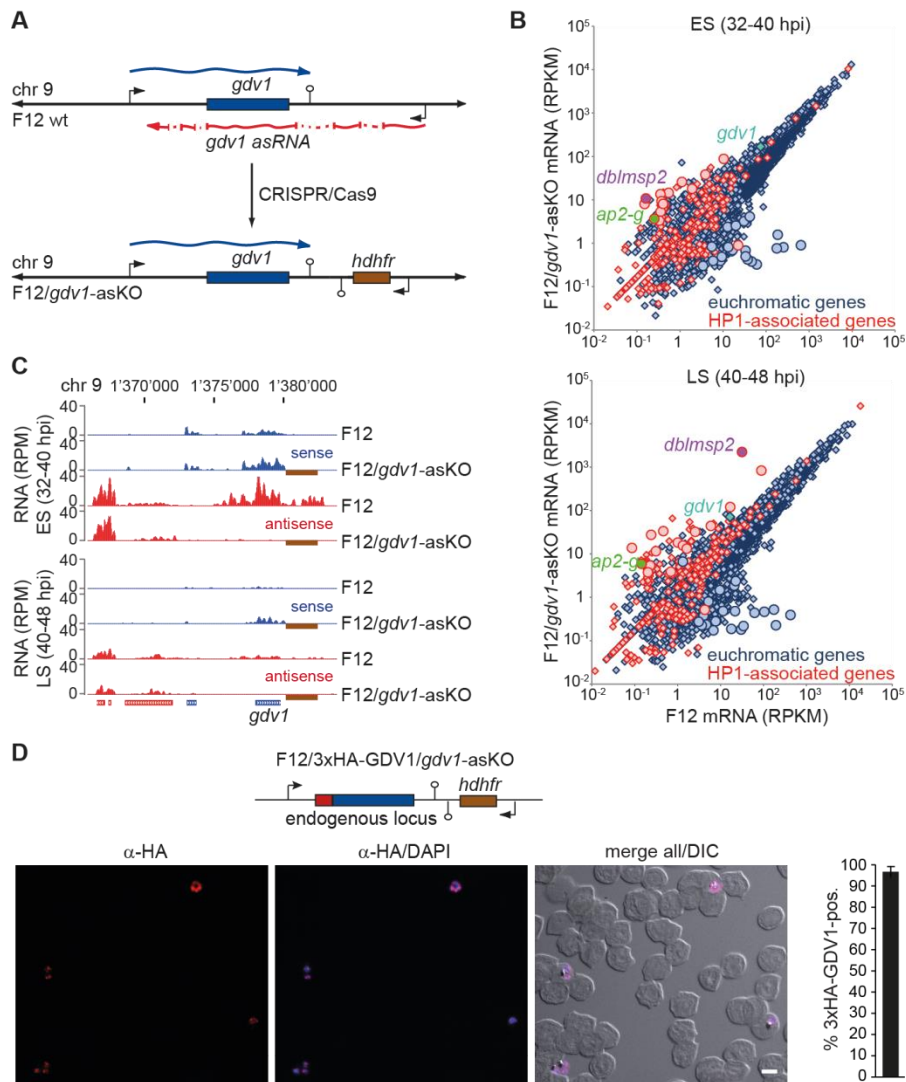


Fig. 4. A *gdv1* antisense RNA antagonises GDV1-dependent sexual commitment. (A) *gdv1* locus in F12 wild-type and F12/*gdv1*-asKO parasites. The *gdv1* sense transcript (blue), five-exon *gdv1*-asRNA (24) (red) and *hdhfr* resistance marker (brown) are highlighted. (B) Comparison of gene expression levels in F12 wild-type and F12/*gdv1*-asKO early (ES) and late (LS) schizonts. Genes de-regulated > 5-fold in both TPs are indicated by circles. (C) UCSC genome browser screenshots of RNA-seq coverage plots over the *gdv1* locus in F12 wild-type and F12/*gdv1*-asKO early (ES) and late (LS) schizonts. The *hdhfr* resistance cassette downstream of the *gdv1* locus in F12/*gdv1*-asKO parasites and absent in the 3D7 reference genome is indicated by a brown box.

(D) Endogenous *gdv1* locus in F12/3xHA-GDV1/*gdv1*-asKO parasites and α -HA overview IFA in early schizonts (ES, 32-40 hpi). DIC, differential interference contrast. Scale bar, 5 μ m. Percentage of 3xHA-GDV1-positive parasites is shown at the right (results are the mean of three biological replicates (100 infected RBCs counted per sample); error bars indicate SD).

Supplementary Materials:

Materials and Methods

Supplementary Text

Figs. S1 to S8

Tables S1 and S2

Captions for Tables S3 to S9

References (33-58)

SUPPLEMENTAL MATERIALS

Materials and Methods

Parasite culture, transfection constructs and transgenic cell lines

P. falciparum 3D7 and F12 parasites were cultured as described (33). Growth synchronization was achieved by repeated sorbitol treatments (34). To generate parasite lines 3D7/GDV1-GFP-DD and F12/GDV1-GFP-DD expressing ectopic GDV1-GFP-DD, the *gdl1* coding sequence (primers *gdl1_pHGFPDD_BamHI* and *gdl1_pHGFPDD_NotI*) was cloned in frame with *gfp-dd* into pHcamGFP-DD using *BamHI* and *SalI*. pHcamGFP-DD was obtained by inserting a PCR fragment encoding the FKBP destabilizing domain (DD) in frame with *gfp* into *SpeI/SalI*-digested pHcamGFP (35). 3D7 and F12 parasites were transfected with pHcamGDV1-GFP-DD and selected with 4nM WR99210 (WR) as described (36). Induction of GDV1-GFP-DD expression was achieved by addition of 312.5 nM Shield-1 to the culture medium unless otherwise indicated.

We generated three new mother plasmids (p_gC, pH_gC and pB_gC) for CRISPR/Cas9-based genome engineering in *P. falciparum* using the following cloning steps. First, plasmid pgRNA was obtained by Gibson assembly joining the *NcoI/PvuII* fragment containing the plasmid backbone and U6 single guide RNA (sgRNA) expression cassette of pL-6_eGFP (37) with a PCR fragment containing a *HindIII-SalI-EcoRI-BamHI* multi-cloning site (MCS) amplified from pET-32a(+) using primers PCR1_F and PCR1_R. In a second step, the *BsaI* site in the *amp^R* gene in pgRNA was eliminated using a Gibson assembly reaction by replacing the 207 bp *BsaI/FspI amp^R* fragment with a corresponding 207 bp PCR fragment obtained with primers PCR2_F and PCR2_R, the latter of which introduced a silent G to A mutation in the *BsaI* recognition sequence (GGTCTC to GATCTC). This plasmid was named pgRNA2. In a third step, the *BtgZI* recognition site in the U6 sgRNA expression cassette in pgRNA2 was replaced with a *BsaI* recognition sequence to obtain pgRNA3. To achieve this, the *BtgZI*-digested pgRNA2 plasmid and a 56 bp fragment obtained by annealing the two complementary oligonucleotides *BsaI_F* and *BsaI_R* were joined by Gibson assembly. In a fourth step, a Cas9 expression cassette was introduced into pgRNA3 using Gibson assembly to obtain the mother plasmid p_gC. Here, *NcoI*-digested pgRNA3 was joined with three PCR fragments amplified from pUF1_Cas9 (37) encoding (1) the *P. falciparum hsp86* promoter (primers PCR4a_F and PCR4a_R), (2) *Streptococcus pyogenes* Cas9 (primers PCR4b_F and PCR4b_R), and (3) the *P. berghei dhfr-ts* terminator (primers PCR4c_F and PCR4c_R). In the fifth step, a human dihydrofolate reductase (hDHFR) resistance cassette was introduced into p_gC by Gibson assembly to obtain the mother plasmid pH_gC. This was achieved by assembling the *BamHI*-digested p_gC with three PCR fragments encoding (1) the *P. falciparum cam* promoter amplified from 3D7 gDNA (primers PCR5a_F and PCR5b_R), (2) the *hdhfr* gene amplified from pL6_eGFP (primers PCR5b_F and PCR5b_R), and (3) the *P. falciparum hrp2* terminator amplified from pL6_eGFP (primers PCR5c_F and PCR5c_R). The mother plasmid pB_gC is a modified version of pH_gC where the hDHFR cassette is replaced with a blasticidin deaminase (BSD) resistance cassette using Gibson assembly. This was achieved by assembling *BamHI/XhoI*-digested pH_gC with three PCR fragments representing (1) the *cam* promoter amplified from pH_gC with primers B1F and B1R; (2) the *bsd* gene amplified from pBcam_3xHA (2) using primers B2F and B2R; and (3) the *hrp2* terminator amplified from pH_gC using primers B3F and B3R. We also generated pHF_gC and pBF_gC, modified versions

of pH_gC and pB_gC, respectively, expressing hDHFR fused to the bifunctional negative selection marker yeast cytosine deaminase/uridyl phosphoribosyl transferase (hDHFR-yFCU) instead of hDHFR alone. For pHF_gC, pH_gC was digested with *XhoI* and *XbaI* (cuts within *hdhfr*) and assembled with four PCR products: (1) the 3' end of *hdhfr* starting at the *XbaI* site amplified from pH_gC using primers HF1F and HF1R; (2) the 5' part of *yfcu* up to the internal *BamHI* site amplified from pL6-eGFP (37) using primers HF2F and HF2R; (3) the 3' part of *yfcu* starting at the internal *BamHI* site amplified from pL6-eGFP (37) using primers HF3F and HF3R (note that the separation of the *yfcu* sequence into two parts was required to eliminate the internal *BamHI* site); and (4) the *hrp2* terminator amplified from pH_gC using primers HF4F and B3R. For pBF-gC, the *BamHI/XhoI*-digested pB_gC vector was assembled with two PCR products: (1) the *cam* promoter and *bsd* coding sequence amplified from pB_gC using primers B1F and BF1R; and (2) the *yfcu* coding sequence and *hrp2* terminator amplified from pHF_gC with primers HF2F and B3R. The mother plasmid p_gC serves as a template to generate CRISPR/Cas9 knockout plasmids (single plasmid approach), and the pH_gC, pB_gC, pHF_gC and pBF_gC mother plasmids are used together with a donor plasmid for gene tagging.

To generate 3D7/AP2-G-GFP-DDglmS parasites we constructed the CRISPR/Cas9 transfection vector pH_gC-*ap2g-3'-gfp-dd-glmS* allowing for marker-free genome editing using a single plasmid. We first generated plasmid pH_gC-*ap2g-3'* by inserting two annealed complementary oligonucleotides (*sgt_ap2g3'_F*, *sgt_ap2g3'_R*) encoding the sgRNA target sequence *sgt_ap2g-3'* and appropriate single-stranded overhangs into the sgRNA expression cassette in pH_gC using *BsaI* digestion and T4 DNA ligase. The sgRNA target sequence *sgt_ap2g3'* (agttatagggaaattcaaa) is positioned 60 bp downstream of the *ap2-g* coding sequence and was identified using CHOPCHOP (38, 39). We then generated a second plasmid carrying an *ap2g-gfp-dd-glmS* donor assembly (pD_*ap2g-gfp-dd-glmS*) using two subsequent cloning steps. First, plasmid pD_*ap2g-gfp* was generated using Gibson assembly joining four PCR fragments encoding (1) the plasmid backbone amplified from pUC19 using primers PCRA_F and PCRA_R, (2) a 393 bp *ap2-g* 5' homology box (HB) (spanning bps 6904-7296 of the *ap2-g* gene) amplified from 3D7 gDNA using primers PCRB_F and PCRB_R, (3) the *gfp* coding sequence (plus N-terminal GSAG linker) amplified from pH-GFP (7) using primers PCRC_F and PCRC_R, and (4) a 670 bp *ap2-g* 3' HB (spanning the region 60-730 bp downstream of the *ap2-g* gene) amplified from 3D7 gDNA using primers PCRD_F and PCRD_R. Second, pD_*ap2g-gfp-dd-glmS* was constructed using Gibson assembly of three PCR fragments representing (1) the *ap2-g* 5' HB/pUC19 backbone/*ap2-g* 3' HB assembly amplified from pD_*ap2g-gfp* using primers 1F and 1R, (2) the *gfp-dd* sequence amplified from pH-GFP-DD (7) using primers 2F and 2R, and (3) the *glmS-246* sequence amplified from pL6-3HA_glmS-246 (kind gift from Dave Richard) using primers 3F and 3R. The final CRISPR/Cas9 transfection vector pH_gC-*ap2g-3'-gfp-dd-glmS* was then obtained by introducing the *EcoRI/HindIII*-digested *ap2g-gfp-dd-glmS* donor assembly amplified from pD_*ap2g-gfp-dd-glmS* (primers EcoF and HindR) into *EcoRI/HindIII*-digested pH_gC-*ap2g-3'*. The pH_gC-*ap2g-3'-gfp-dd-glmS* construct was transfected into 3D7 parasites and 3D7/AP2-G-GFP-DDglmS parasites were selected with 4 nM WR and 2.5 mM (D)- α -glucosamine (GlcN) (Sigma Aldrich) for six days and then maintained in absence of WR until a stably propagating parasite population was established. Successful editing of the *ap2-g* locus was confirmed by PCR on gDNA. Stabilisation of AP2-G-GFP-DD expression was achieved by removing GlcN and adding 1350 nM Shield-1 to the culture medium.

To disrupt the antisense RNA locus downstream of the *gdv1* coding sequence in F12 wild-type and 3D7/AP2-G-GFP-DDglmS parasites we generated the CRISPR/Cas9 knockout vectors p_gCH-*gdv1-asKO* and p_gCB-*gdv1-asKO*, respectively. First, p_gC-*gdv1-asKO-pre* was

created by inserting a *hdhfr* resistance cassette flanked by the 5' and 3' HBs into p_gC using Gibson assembly. This was achieved by assembling *EcoRI/HindIII*-digested p_gC with three PCR fragments encoding (1) a 440 bp 5' HB amplified from 3D7 gDNA (spanning the last 93 bp of the *gdv1* coding sequence and 347 bp of the downstream sequence; primers p_gC-*gdv1*-asKO_5'HB_for and p_gC-*gdv1*-asKO_5'HB_rev), (2) a *hdhfr* resistance cassette amplified from pH_gC (primers p_gCH-*gdv1*-asKO_5'HB_for and p_gCH-*gdv1*-asKO_5'HB_rev), and (3) a 753 bp 3' HB amplified from 3D7 gDNA (spanning the region 3,554-4,307 bp downstream of the *gdv1* coding sequence; primers p_gCH-*gdv1*-asKO_3'HB_for and p_gCH-*gdv1*-asKO_3'HB_rev). To generate the final p_gCH-*gdv1*-asKO construct, the two complementary oligonucleotides (sgt_*gdv1*-3'_F and sgt_*gdv1*-3'_R) encoding the sgRNA target sequence sgt_*gdv1*-3' and appropriate single-stranded overhangs were annealed and inserted into the sgRNA expression cassette using *BsaI*-digested p_gC-*gdv1*-asKO-pre and T4 DNA ligase. The sgRNA target sequence sgt_*gdv1*-3' (tgtattactaaagaatgaaa) is positioned 1,639 bp downstream of the *gdv1* coding sequence and was identified using CHOPCHOP (38, 39). For the p_gCB-*gdv1*-asKO construct, p_gCH-*gdv1*-asKO was cut with *XhoI* and *EcoRI* to release the *hdhfr* resistance cassette and the 3' HB. Gibson assembly was then used to insert PCR fragments encoding the blasticidin deaminase (*bsd*) resistance cassette amplified from pB_gC (primers p_gCB-*gdv1*-asKO_for and p_gCB-*gdv1*-asKO_rev) and the identical 753 bp 3'HB amplified from 3D7 gDNA (primers p_gCB-*gdv1*-asKO_3'HB_for and p_gCB-*gdv1*-asKO_3'HB_rev). The p_gCH-*gdv1*-asKO construct was transfected into F12 parasites and F12/*gdv1*-asKO parasites were selected with 4 nM WR. The p_gCB-*gdv1*-asKO construct was transfected into 3D7/AP2-G-GFP-DDglmS parasites grown in presence of 2.5 mM GlcN and 3D7/AP2-G-GFP-DDglmS/*gdv1*-asKO parasites were selected with 2.5 µg/ml blasticidin-S-HCl (BSD). Successful disruption of the *gdv1*-asRNA locus and replacement with the *hdhfr* or *bsd* resistance cassettes was confirmed by PCR on gDNA. Stabilisation of AP2-G-GFP-DD expression was achieved by removing GlcN and adding 1350 nM Shield-1 to the culture medium.

To create the 3D7/3xHA-GDV1 and F12/3xHA-GDV1/*gdv1*-asKO parasite lines we prepared the CRISPR/Cas9 transfection vectors pB_gC-*gdv1*-5' and the donor plasmid pFDon_3xha-*gdv1*. pFDon contains an expression cassette for *yfcu* under control of the *hsp86* promoter and was cloned by Gibson assembly of four PCR fragments: (1) the pUC18 *E. coli* plasmid backbone amplified with primers D1F and D1R; (2) the *hsp86* promoter amplified from pHF_gC using primers D2F and D2R; (3) the *yfcu* coding sequence and *hrp2* terminator amplified from pHF_gC using primers D3F and D3R; and (4) the MCS amplified from pHF_gC using primers D4F and D4R. To obtain pFDon_3xha-*gdv1*, three PCR fragments were inserted into the pFDon plasmid by Gibson assembly: (1) a 5' HB spanning 504 bp of the *gdv1* upstream region (-505 to -1) amplified from 3D7 gDNA (primers pFDon_GDV1_HA_for and pFDon_GDV1_HA_rev); (2) a 93 bp fragment coding for a 3xHA-tag amplified from pBcam_3xHA (primers pFDon_GDV1_HA_HAtag_for and pFDon_GDV1_HA_HAtag_rev); and (3) a 3' HB spanning 488 bp of the *gdv1* coding region (+3 to +491) amplified from 3D7 gDNA. The 3' HB fragment was created in a two-step process. First, a fragment containing three mismatch mutations in the sgRNA target sequence sgt_*gdv1*-5' (tgaaagtaaaaggtaatagt to tgaaGgtTaaaggCaatagt) was amplified from 3D7 gDNA (primers pFDon_GDV1_HA_3'HB_mut_for and pFDon_GDV1_HA_3'HB_mut_rev). This sequence was then used as template for a second round of amplification adding overhangs for Gibson assembly (primers pFDon_GDV1_HA_3'HB_for and pFDon_GDV1_HA_3'HB_rev). To create the pB_gC-*gdv1*-5' CRISPR/Cas9 plasmid two complementary oligonucleotides (sgt_*gdv1*-5'_F and sgt_*gdv1*-5'_R) encoding the sgRNA target sequence sgt-*gdv1*-5' (tgaaagtaaaaggtaatagt;

positioned 28 bp downstream of the start codon of the *gdv1* coding sequence) were annealed and inserted into the *BsaI* site in pB_gC. Equal amounts of both plasmids were transfected into 3D7 wild-type and F12/*gdv1*-asKO parasites and 3D7/3xHA-GDV1 and F12/3xHA-GDV1/*gdv1*-asKO parasites were selected with 5 µg/ml BSD for 10 days and then maintained in absence of drug pressure until stably propagating parasite populations were established. Successful editing of the *gdv1* locus was confirmed by PCR on gDNA. The 3D7/3xHA-GDV1 line was cloned out as described (40).

All oligonucleotide sequences used for cloning and confirmation of CRISPR/Cas9-based gene editing by PCR are provided in Table S9.

Preparation of parasite nuclear extracts

Nuclei were isolated as described (41). Prior to nuclear protein extraction, nuclei were treated with DNase I and RNase A (20mM Hepes pH 7.4, 10mM NaCl, 5mM MgCl₂, 1mM CaCl₂, 0.1% NP-40, 1x protease inhibitor (Roche Diagnostics), 1x PhosSTOP (Roche Diagnostics), 0.5 U/µl DNase I (Roche Diagnostics), 1µg RNase A (Roth)) in a 250 µl reaction for 5min at 37°C. Reactions were adjusted to 500 µl using 2x high salt extraction buffer (20mM Hepes pH 7.4, 1M NaCl, 6mM EDTA, 2mM EGTA, 2mM TCEP, 1x protease inhibitor (Roche Diagnostics), 1x PhosSTOP (Roche Diagnostics), 50% Glycerol, 0.1%NP-40) and nuclear proteins were extracted in 2.5 pellet volumes high salt extraction buffer (20mM Hepes pH 7.4, 500mM NaCl, 3mM EDTA, 1mM EGTA, 1mM TCEP, 1x protease inhibitor (Roche Diagnostics), 1x PhosSTOP (Roche Diagnostics), 25% Glycerol, 0.1%NP-40) containing 0.02mg/ml H3K9me3 peptides (Diagenode) and incubated at 4°C for 1 h. After centrifugation at 20800g at 4°C for 30min supernatants were immediately used for co-IP experiments.

Co-Immunoprecipitation (co-IP)

High salt nuclear extract from 3D7/HP1-GFP or 3D7/GDV1-GFP-DD^{ON} schizonts was diluted to 250mM NaCl using dilution buffer (20mM Hepes pH 7.4, 1mM EDTA, 1mM TCEP, 1x protease inhibitor (Roche Diagnostics), 1x PhosSTOP (Roche Diagnostics), 25% Glycerol) and incubated with negative control agarose beads (Chromotek) for 30 min at 4°C under constant agitation for lysate pre-clearing. The supernatant was split and incubated with GFP-Trap agarose beads (Chromotek) or negative control agarose beads (Chromotek) for 1 h at 4°C under constant agitation. The supernatant was recovered and beads were washed four times in wash buffer 1 (20mM Hepes pH 7.4, 250mM NaCl, 1mM EDTA, 1mM TCEP, 0.05% NP-40) and once in wash buffer 2 (20mM Hepes pH 7.4, 250mM NaCl, 1mM EDTA, 1mM TCEP). Bound proteins were eluted for 1 h at RT under constant agitation using 2M arginine buffer (2M arginine, pH 4) followed by a second elution in 2% SDS buffer (2% SDS, 20mM Tris-HCl, pH 8) for 10 min at 95°C. All centrifugation steps were performed at 4°C for 3 min at 500g. Samples were analysed by Western blot using mouse mAb α-GFP (Roche Diagnostics #11814460001) or rabbit α-PfHP1 (7) antibodies.

Capillary liquid chromatography-tandem mass spectrometry (LC-MS/MS)

For the HP1 co-IP experiments, both the 2M arginine elution and the 2% SDS elution were analysed by LC-MS/MS. For the GDV1-GFP-DD co-IP experiments only the 2% SDS elution samples were analysed. Proteins in the 2M arginine elution buffer were reduced with 10 mM DTT at 37°C for 1 hr and alkylated with 50 mM iodo-acetamide for 15 min at room temperature. Proteins were digested with 250 ng endoproteinase LysC (Wako, Neuss, Germany) for two hours

at 37°C followed by 500 ng trypsin (Worthington, Lakewood, NJ, USA) overnight. The digest was stopped with 1% TFA and desalted on a microspin column (The Nest Group, Southborough, MA, USA) according to the manufacturer's recommendations. Proteins eluted with 2% SDS were precipitated with 10% TCA, washed twice in ice-cold acetone and air-dried. The protein pellets were dissolved in 30 µl 100 mM Tris-HCl (pH 8.0)/6M Urea, containing 10 mM DTT and reduced, alkylated and digested with 250 ng endoproteinase LysC as above. The urea concentration was diluted to 2 M with 100 mM Tris-HCl (pH 8.0) and the sample was further digested with 500 ng trypsin overnight at 37°C. The digest was acidified with 1% TFA and the sample was desalted on a MicroSpin cartridge.

The peptides were dried in a SpeedVac and dissolved in 40 µL 0.1% formic acid and analysed by capillary liquid chromatography tandem MS (LC-MS/MS) using a home-packed separating column (0.075 mm x 15 cm) packed with Reprosil C18 reverse-phase material (2.4 µm particle size, Dr. Maisch, Ammerbuch-Entringen, Germany). The column was connected on line to an Orbitrap Elite FT hybrid instrument (Thermo Scientific, Reinach, Switzerland). The solvents used for peptide separation were 0.1% formic acid in water/0.005% TFA (solvent A) and 0.1% formic acid/0.005% TFA and 80% acetonitrile in water (solvent B). 2 µl of peptide digest were injected with a Proxeon nLC capillary pump (Thermo Scientific) set to 0.3 µl/min. A linear gradient from 0 to 40% solvent B in solvent A in 95 min was delivered with the nano pump at a flow rate of 300 nl/min. After 95 min the percentage of solvent B was increased to 75% in ten minutes. The eluting peptides were ionized at 2.5 kV. The mass spectrometer was operated in data-dependent mode. The precursor scan was done in the Orbitrap set to 60,000 resolution, while the fragment ions were mass analyzed in the LTQ instrument. A top twenty method was run so that the twenty most intense precursors were selected for fragmentation. The MS/MS spectra were searched against a combined *P. falciparum* (www.plasmoDB.org; release 11.1)/human annotated protein database using Proteome Discoverer 1.4 (Thermo Scientific, Reinach, Switzerland) using the two search engines Mascot and SequestHT (Tables S3 and S4). For the search, oxidized methionine and N-terminal protein acetylation were used as variable modifications. The identifications were filtered to a peptide false discovery rate of 1%.

Fluorescence microscopy

IFAs were performed with methanol-fixed or 4% formaldehyde/0.0075% glutaraldehyde-fixed cells using the following primary antibodies: mouse mAb α-GFP (Roche Diagnostics #11814460001), 1:100; rat mAb α-HA (3F10, Roche Diagnostics #11867423001), 1:100; rabbit α-PfHP1 (7), 1:200; mouse mAb α-Pfs16 (kind gift from Robert W. Sauerwein), 1:500. Secondary antibodies: Alexa Fluor 568-conjugated α-rabbit IgG (Molecular Probes #A11011), 1:500; Alexa Fluor 488-conjugated α-rabbit IgG (Molecular Probes #A11008), 1:500; Alexa Fluor 488-conjugated α-mouse IgG (Molecular Probes #A11001), 1:500; Alexa Fluor 488-conjugated α-rat IgG (Molecular Probes #A11006), 1:250; Alexa Fluor 568-conjugated α-rat IgG (Molecular Probes #A11077), 1:250. Nuclei were stained with DAPI. Images were taken on a Leica DM 5000B microscope with a Leica DFC 345 FX camera, acquired via the Leica IM1000 software, and processed using Fiji (42). For each experiment, images were acquired and processed with identical settings.

Western Blot

Parasites were released from infected RBCs by saponin lysis, resuspended in 8M Urea, 5%SDS, 40mM Tris pH 6.8, 1% β-Mercaptoethanol, 1x protease inhibitor (Roche Diagnostics)

and separated on NuPage 4-12% Bis-Tris gels (Novex). Proteins were detected with mouse mAb α -GFP (Roche Diagnostics #11814460001), 1:500; rabbit α -PfHP1 (7), 1:5'000; mouse mAb α -PfGAPDH (43), 1:20'000; rat mAb α -HA (3F10, Roche Diagnostics #11867423001), 1:10'000; mouse mAb α -6xHIS (R&D Systems #MAB050R), 1:5'000.

In vitro protein-protein interaction experiments

A plasmid vector with the following expression cassette was constructed for co-expression of HP1 and GDV1: T7 promoter/*strep(II)-hp1*/T7 promoter/*6xhissumo-gdv1*/T7 terminator (pStrep-HP1_HS-GDV1). We used pETA-HS and pETA-Strep as parental vectors, which we previously constructed for the expression of N-terminal 6xHis-SUMO-tagged and N-terminally Strep(II)-tagged fusion proteins, respectively. pETA-HS was obtained by introducing a sequence encoding a 6xHis stretch followed by *Saccharomyces cerevisiae* SUMO (amplified from gDNA using primers SUMO_F and SUMO_R between the *NdeI* and *BamHI* sites of pET20(b)+ (Novagen), yielding a vector similar to the one described elsewhere (44). pETA-Strep was generated by replacing the *NdeI/BamHI* fragment in pET20b(+) with an annealed double-stranded oligonucleotide (Strep_F and Strep_R) encoding Met-Ala-Ser-Strep(II). The co-expression plasmid pStrep-HP1_HS-GDV1 was cloned by Gibson assembly of four PCR products representing (1) the backbone of pETA-Strep amplified using the primers SF and SR; (2) the *hp1* coding sequence (cds) starting at +4 amplified from 3D7 gDNA using primers HP1F and HP1R; (3) the T7 promoter and the sequence encoding the 6xHis-SUMO tag amplified from pETA-HS with primers HSF and HSR; and (4) the *gdv1* cds starting at +4 amplified from 3D7 gDNA using primers GDV1F and GDV1R. A control vector with the same expression setup was made by replacing the *gdv1* cds with a fragment encoding amino acids M173 to N311 of the ApiAP2 DNA-binding protein SIP2 (45). This fragment was first ligated into pETA-HS (resulting in pETA-HS-SIP2) using the *SfoI* and *XhoI* restriction sites and the *XhoI*-digested *sip2* PCR product amplified from 3D7 gDNA with primers SIP2F and SIP2R. Next, the pStrep-HP1_HS-SIP2 co-expression vector was Gibson assembled using two PCR products representing (1) the pStrep-HP1_HS-GDV1 vector omitting the *gdv1* cds (amplified using primers SHHSF and SHHSR); and (2) the *sip2* cds fragment amplified from pETA-HS-SIP2 using primers SIP2F2 and SIP2R2. After cloning in *E. coli* DH5alpha and DNA sequencing, the plasmids were transformed into Rosetta2(DE3) cells (Novagen) for recombinant protein expression.

Recombinant proteins were expressed by auto-induction at 25°C (46). Once the cultures were grown to saturation, the bacteria were spun down and pellets frozen. Stock solutions for chromatography were 3 M arginine phosphate (3 M L-arginine, 1.6 M H₃PO₄, pH 7.3), 4 M imidazole phosphate (4 M imidazole, 0.888 M H₃PO₄), 4 M ammonium phosphate (2.8 M (NH₄)₂HPO₄, 1.2 M (NH₄)H₂PO₄). Recombinant proteins were purified using the following strategy: (1) nickel affinity purification: bacterial pellets were thawed, resuspended in buffer Ni-A (200 mM arginine phosphate, 500 mM NaCl, 20 mM imidazole phosphate, 5 mM 6-aminocaproic acid, 0.5 mM TCEP, pH 7.2) and lysed by sonication. The lysate was cleared by centrifugation and loaded on a 5 ml HisTrap HP column (GE-Healthcare). The column was washed with 15 column volumes (CV) of buffer Ni-A and the proteins were eluted using five CV-long linear gradient of Ni-A to Ni-B (Ni-A with 400 mM imidazole phosphate). Both the Strep(II)-HP1/HisSUMO-GDV1 complex and HisSUMO-SIP2 eluted in the same range of the gradient. (2) StrepTactin affinity purification: the nickel column elution obtained from the GDV1/HP1 lysate was loaded on a 5 ml StrepTrap HP column (GE Healthcare), washed with ten CV of buffer Strep-A (200 mM arginine phosphate, 300 mM ammonium phosphate, 30 mM

NaOH, 5 mM 6-aminocaproic acid, 1 mM EDTA, 0.5 mM TCEP, pH 7.4) and eluted using buffer Strep-B (400 mM arginine phosphate, 300 mM ammonium phosphate, 5 mM 6-aminocaproic acid, 1 mM EDTA, 2.5 mM desthiobiotin, 0.5 mM TCEP, pH 7.4). To purify Strep(II)-HP1 without interaction partner, the nickel column flow through obtained from the SIP2-HP1 control lysate was used and purified using the same conditions. (3) Hydrophobic interaction chromatography: the salt concentration of the StrepTactin column elutions were adjusted to 0.75 M ammonium phosphate and loaded on a 1 ml Phenyl HP column (GE Healthcare). The column was washed using ten CV of buffer HIC-A (400 mM arginine phosphate, 750 mM ammonium phosphate, 5 mM 6-aminocaproic acid, 1 mM EDTA, 0.5 mM TCEP, pH 7.2) and the proteins were eluted using a 25 CV-long linear gradient of buffer HIC-A to HIC-B (400 mM arginine phosphate, 5 mM 6-aminocaproic acid, 1 mM EDTA, 50 % (w/v) ethylene glycol, 0.5 mM TCEP, pH 7.2). The Strep(II)-HP1/HisSUMO-GDV1 complex was concentrated using an Amicon spin filter (Millipore) with a 10 K cut-off. Protein samples were analysed by SDS/polyacrylamide gel electrophoresis followed by Coomassie staining or Western blot analysis.

All oligonucleotide sequences used for cloning of expression vectors are provided in Table S9.

Gametocyte conversion, differentiation and sex ratios

To quantify sexual conversion rates of 3D7/GDV1-GFP-DD parasites, synchronous 3D7/GDV1-GFP-DD^{OFF} cultures were split at 8-16 hours post-invasion and one half was maintained in the absence of Shield-1 and one half was cultured in the presence of Shield-1 (3D7/GDV1-GFP-DD^{ON}). After re-invasion, parasites were fixed at 38-46 hpi either with methanol (Fig. 2B) or 4% formaldehyde/0.0075% glutaraldehyde (Fig. S2) and α -Pfs16 IFAs combined with DAPI staining was performed to quantify sexual conversion rates (proportion of stage I gametocytes among all infected RBCs). To assess gametocyte differentiation, cultures were treated with 50 mM N-acetyl-D-glucosamine (GlcNAc) for the first four days after re-invasion to eliminate asexual parasites (47) and then with normal culture medium for another 4-6 days when mature stage V gametocytes were observed in Giemsa-stained thin blood smears.

To quantify male and female gametocytes synchronous 3D7/GDV1-GFP-DD^{OFF} cultures were split at 8-16 hours post-invasion and one half was maintained in the absence of Shield-1 while the other half was cultured in the presence of Shield-1 (3D7/GDV1-GFP-DD^{ON}). After re-invasion, parasites were treated with 50 mM GlcNAc as above. Gametocytaemia was determined four days after re-invasion by visual inspection of Giemsa-stained blood smears and used to calculate the sexual conversion rate (gametocytaemia observed on day four in relation to the total parasitaemia observed on day one after re-invasion). Eleven days after re-invasion male and female gametocytes were quantified by inspection of Giemsa-stained blood smears as described elsewhere (48) (for each population three individual blood smears were scored blindly).

To assess 3xHA-GDV1 expression under growth conditions that either suppress or induce sexual commitment, 3D7/3xHA-GDV1 parasites were split at 24-30 hours post-invasion and pulsed with defined minimal fatty acid medium (RPMI-1640 medium, 25 mM HEPES, 24 mM sodium bicarbonate, 100 μ M hypoxanthine, 0.39% fatty acid-free BSA (Sigma-Aldrich), 30 μ M oleic acid, 30 μ M palmitic acid), either supplemented with 2 mM choline (suppresses sexual commitment) or lacking choline (induces sexual commitment), respectively (16). Twelve hours after pulsing relative 3xHA-GDV1 expression levels were determined by Western blot and IFAs were performed to determine the proportion of parasites expressing 3xHA-GDV1 in haemozoin-

positive parasites (1n-4n). Sexual conversion rates were determined as described above by visual inspection of Giemsa-stained blood smears after GlcNAc treatment.

To quantify sexual conversion rates of 3D7/AP2-G-GFP-DDglmS and 3D7/AP2-G-GFP-DDglmS/*gdl1*-asKO parasites, synchronous cultures were split at 24-32 hours post-invasion and one half was maintained in the presence of glucosamine/absence of Shield-1 and one half was cultured in the absence of glucosamine/presence of Shield-1. Sexual conversion rates were determined as described above by α -Pfs16 IFAs on methanol-fixed thin smears.

Chromatin immunoprecipitations, high throughput sequencing and data analysis

3D7/GDV1-GFP-DD^{OFF} parasites were synchronized twice 18 hours apart to obtain a six hour growth window (18-24 hpi). At 28-34 hpi cultures were split and one half was maintained in the absence of Shield-1 and one half was cultured in the presence of Shield-1 (3D7/GDV1-GFP-DD^{ON}). Paired samples of 3D7/GDV1-GFP-DD^{OFF} and 3D7/GDV1-GFP-DD^{ON} parasites were harvested at three consecutive time points (TPs) two (30-36 hpi, TP1), six (34-40 hpi, TP2) and ten (38-44 hpi, TP3) hours after addition of Shield-1 by crosslinking with 1% formaldehyde for 15 min at 37°C. The crosslinking reaction was quenched by 0.125 M glycine. Nuclei were isolated by releasing parasites from infected RBCs using 0.05% saponin followed by lysis in CLB (20 mM Hepes, 10 mM KCl, 1 mM EDTA, 1 mM EGTA, 0.65% NP-40, 1 mM DTT, 1x protease inhibitor (Roche Diagnostics)). Nuclei were washed and snap-frozen in CLB supplemented with 50% glycerol. Nuclei were resuspended in sonication buffer (50 mM Tris pH 8, 1% SDS, 10 mM EDTA, 1x protease inhibitor (Roche Diagnostics)) and sonicated for 20 cycles of 30 sec ON/30 sec OFF (setting high, BioruptorTM Next Gen, Diagenode). Fragment sizes ranged from 100-600 bp as determined by de-crosslinking a 50 μ l aliquot and running the purified DNA on a 1% agarose gel. ChIPs were performed under rotation overnight at 4°C in incubation buffer (5% Triton-X-100, 750 mM NaCl, 5 mM EDTA, 2.5 mM EGTA, 100 mM Hepes pH 7.4) by combining sonicated chromatin (500 ng DNA content) with either 1 μ g mouse mAb α -GFP (Roche Diagnostics #11814460001) or 1 μ g rabbit α -PfHP1 (7) in the presence of 10 μ l protA and 10 μ l protG Dynabeads (Life Technologies, #10008D and #10009D). Beads were washed for 5 min at 4°C while rotating with 400 μ l of the following wash buffers: 2x wash buffer 1 (0.1% SDS, 0.1% DOC, 1% Triton-X100, 1 mM EDTA, 0.5 mM EGTA, 20 mM Hepes pH 7.4), 1x wash buffer 2 (0.1% SDS, 0.1% DOC, 1% Triton-X100, 500 mM NaCl, 1 mM EDTA, 0.5 mM EGTA, 20 mM Hepes pH 7.4), 1x wash buffer 3 (250 mM LiCl, 0.5% DOC, 0.5% NP-40, 1 mM EDTA, 0.5 mM EGTA, 20 mM Hepes pH 7.4), 2x wash buffer 4 (1 mM EDTA, 0.5 mM EGTA, 20 mM Hepes pH 7.4). The immunoprecipitated chromatin was eluted in 200 μ l elution buffer (1% SDS, 0.1 M NaHCO₃) while rotating for 20 min at RT and de-crosslinked (1% SDS, 0.1 M NaHCO₃, 1 M NaCl) in a 45°C shaking heat-block overnight. In parallel, 30 μ l of sonicated input chromatin was de-crosslinked under the same conditions. The DNA was purified using QIAquick MinElute PCR columns (Qiagen) and eight separate α -GFP ChIPs or four separate α -PfHP1 ChIPs were combined.

To prepare sequencing libraries 1 ng of input DNA, 1 ng α -GFP ChIP DNA or 5 ng α -HP1 ChIP DNA were end repaired, extended with 3' A-overhangs and ligated to barcoded NextFlex adapters (Bio Scientific, #514122) as described (49). Libraries were amplified using an optimized KAPA protocol (50) using KAPA HiFi HotStart ready mix (KAPA Biosystems, KM2602), NextFlex primer mix (Bio Scientific, #514122) and the following PCR program: 98°C for 2 min; four cycles of 98°C for 20 sec, 62°C for 3 min; 62°C for 5 min. Amplified libraries were size-selected for 225-325 bp (mono-nucleosomes + 125 bp NextFlex adapter) using 2% E-Gel Size

Select agarose gels (Invitrogen, #G6610-02) and amplified by PCR for ten cycles using the above conditions. Libraries were purified and adapter dimers removed by Agencourt AMPure XP beads purification using a 1:1 library:beads ratio (Beckman Coulter, #A63880). ChIP-seq libraries were sequenced on the Illumina NextSeq 500 system to generate 75 bp single-end reads (NextSeq 500/550 High Output v2 kit). Reads were mapped against the *P. falciparum* 3D7 reference genome from PlasmoDB v26 (www.plasmodb.org) using BWA samse (v0.7.12-r1039) and filtered to mapping quality ≥ 15 (SAM tools v1.2). Only uniquely mapped reads (between 3.7 and 11.5 million reads) were used for further analysis.

To visualize ChIP-seq data in the UCSC Genome browser, all libraries were normalized to the amount of mapped reads per million (RPM). Bedgraph files were generated using bedtools (v2.20.1). For log₂ ratio tracks HP1 or GDV1-GFP-DD ChIP values were divided by input values and log₂-transformed. For subtraction tracks ChIP values obtained from 3D7/GDV1-GFP-DD^{OFF} parasites were subtracted from those obtained from 3D7/GDV1-GFP-DD^{ON} parasites. Within the UCSC genome browser tracks were smoothed (10-16) and the windowing function was set as 'mean'. To assess HP1 and GDV1-GFP-DD coverage of individual genes, tags were counted for each coding region and offset by +1 to avoid division by zero while calculating fold change in coverage. Coding region counts were normalized to the number of reads per kb per million mapped reads (RPKM). Genes with very low mapability (input RPKM < 5) were excluded from further analysis. ChIP-seq enrichment values (ChIP/input) were calculated over each coding region.

Microarray experiments and data analysis

3D7/GDV1-GFP-DD^{OFF} parasites were synchronized twice 16 hours apart to obtain an eight hour growth window (16-24 hpi). After re-invasion parasites were synchronised again at 0-8 hpi. At 4-12 hpi the culture was split and one half was maintained in the absence of Shield-1 and one half was cultured in the presence of Shield-1 (3D7/GDV1-GFP-DD^{ON}). For both populations, total RNA was isolated in the same cell cycle (generation 1) from trophozoites (T1; 24-32 hpi), early schizonts (ES1; 32-40 hpi), late schizonts (LS1; 40-48 hpi), and after re-invasion (generation 2) from early ring stages (ER2; 8-16 hpi), late ring stages (LR2; 16-24 hpi), trophozoites (T2; 24-32 hpi), early schizonts (ES2; 32-40 hpi). Corresponding samples of F12/GDV1-GFP-DD^{OFF} and F12/GDV1-GFP-DD^{ON} parasites were prepared accordingly. RNA extraction and cDNA synthesis was carried out as described (51). Cy5-labelled test cDNAs were hybridised against Cy3-labelled cDNA reference pool consisting of total RNA obtained from 3D7 wild-type parasites harvested at five consecutive TPs along intra-erythrocytic parasite development (7). Equal amounts of Cy5- and Cy3-labelled samples were hybridised on a *P. falciparum* 8×15K Agilent gene expression microarray (GEO platform ID GPL15130) for 16 hours at 65°C in an Agilent hybridisation oven (G2545A) (52). Slides were scanned using the GenePix scanner 4000B and GenePix pro 6.0 software (Molecular Devices). The raw microarray data representing relative transcript abundance ratios between each test sample and the reference pool (Cy5/Cy3 log₂ ratios) were subjected to lowess normalization and background filtering as implemented by the Acuity 4.0 program (Molecular Devices). Flagged features and features with either Cy3 or Cy5 intensities lower than two-fold the background were discarded. Log₂ ratios for multiple probes per gene were averaged. Transcripts showing expression values at all seven consecutive paired time points were included for downstream analysis. We performed paired two-class Significance Analysis of Microarrays (SAM) (53) to identify genes with significant differential expression between 3D7/GDV1-GFP-DD^{OFF} and 3D7/GDV1-GFP-DD^{ON} or F12/GDV1-GFP-DD^{OFF} and F12/GDV1-GFP-DD^{ON} parasites, respectively (q-value (fdr) cut-off

<0.15; mean fold change cut-off >1.5). Heatmaps were generated using Java Treeview (54). Scatterplots were generated using Microsoft Excel. The processed microarray data are listed in Table S5 (3D7/GDV1-GFP-DD) and S6 (F12/GDV1-GFP-DD).

RNA-seq library preparation, high throughput sequencing and data analysis

F12 and F12/*gdv1*-asKO parasites were synchronized twice 16 hours apart to obtain an eight hour growth window. Parasites were harvested at 32-40 hpi and at 40-48 hpi. Total RNA was isolated using Ribozol (Amresco) according to the manufacturer's manual and further purified using the RNeasy Plus Mini Kit (Qiagen) for removal of gDNA. Residual gDNA was digested with TURBO DNA-freeTM DNaseI (Ambion) and the RNA was quantified by NanoDrop. Total RNA was polyA-selected using the Oligotex mRNA Mini Kit (Qiagen, #70022) according to manufacturer's instructions. Subsequently, 2 µg of polyA-selected total RNA equivalent were fragmented by alkaline hydrolysis (5x fragmentation buffer: 200 mM Tris-acetate pH 8.2, 500 mM potassium acetate, 150 mM magnesium acetate) for 1 min 45 sec at 85°C in a 150 µl volume and precipitated as previously described (55), followed by two TURBO DNase treatments (Ambion, #AM2238) to remove possible remnants of genomic DNA. Further library preparation for strand-specific RNA-seq was carried out as described (50). In short, first-strand cDNA synthesis was performed with AT-corrected random N9 primers (76% AT) in presence of 0.2 µg Actinomycin D (Thermo 446 Fisher Scientific) to prevent DNA-dependent second-strand cDNA synthesis. To maintain the strand-specific information during second-strand synthesis dTTPs were replaced with dUTPs. Resulting double-stranded cDNAs (1.9-3.2 ng) were end-repaired and extended with 3' A-overhangs. After ligation of NextFlex adapters (Bio Scientific, #514122), libraries were treated with USER enzyme (NEB, #M5505L) to specifically degrade the dUTP-containing second strand and subsequently amplified by PCR (98°C for 2 min; 4 cycles of 98°C for 20 sec, 62°C for 3 min; 62°C for 5 min) using KAPA HiFi HotStart ready mix (KAPA Biosystems, #KM2602) and NEXTflex primer mix (Bio Scientific, #514122). Next, libraries were size-selected for 300-400 bp fragments using 2% E-Gel Size Select agarose gels (Invitrogen, #G6610-02) and amplified for another 12 cycles using the same conditions as above. Subsequent depletion of adapter dimers and library purification was performed using Agencourt AMPure XP beads (Beckman Coulter, #A63880) in a 1:1 library beads ratio.

Strand-specific RNA-seq libraries were sequenced on the Illumina NextSeq 500 system to generate 75 bp single-end reads (TruSeq SR Cluster Kit v2), which were mapped against the *P. falciparum* 3D7 transcriptome from PlasmoDB v26 using BWA samse (version 0.7.12-r1039). Reads were filtered for mapping quality ≥ 15 (samtools version 1.2) and only uniquely mapped reads (between 1.6 and 4.7 million reads) were used for further analysis. After separating the reads according to the strand they mapped to (sense strand FLAG16, antisense strand FLAG0), sense and antisense transcript abundance was assessed by counting the respective tags for each transcript except for transcripts originating from the mitochondrial and apicoplast genomes. Resulting tag counts were offset by +1 and normalized to the number of reads per kb per million mapped reads (RPKM). RPKM ratios were calculated when at least one of the two samples per time point had a RPKM value ≥ 3 . To visualize RNA-seq data in the UCSC Genome browser, 75 bp reads were additionally mapped against the annotated *P. falciparum* 3D7 genome (PlasmoDB v26), filtered as described above and split into reads mapping to the sense strand (FLAG16) and antisense strand (FLAG0), respectively. RNA-seq libraries were normalized to the number of mapped reads per million (RPM) and bedgraph files were generated (bedtools v2.20.1). After

uploading the tracks to the UCSC genome browser, tracks were smoothed (5) and the windowing function was set as 'mean'.

Reverse transcription quantitative PCR (RT-qPCR)

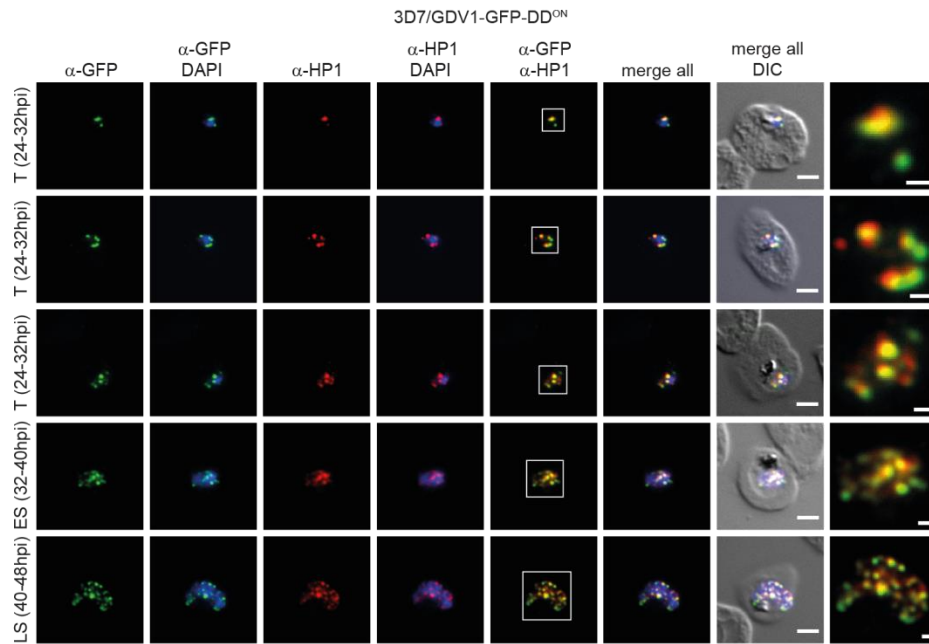
F12 and F12/*gdv1*-asKO parasites were synchronized twice 16 hours apart to obtain an eight hour growth window. Parasites were harvested at 40-48 hpi. Total RNA was isolated using Ribozol (Amresco) according to the manufacturer's manual and further purified using the RNeasy Plus Mini Kit (Qiagen) for removal of gDNA. Residual gDNA was digested with TURBO DNA-free™ DNaseI (Ambion) and the RNA was quantified by NanoDrop. All samples were tested negative for contaminating gDNA by qPCR. 2 µg total RNA was reverse-transcribed using the RETROscript Kit (Ambion). qPCR reactions were performed at primer concentrations of 0.5 µM using Power SYBR® Green PCR Master Mix (Applied Biosystems) on a StepOnePlus™ Real-Time PCR System (Applied Biosystems) in a reaction volume of 20 µl. All reactions were run in triplicate yielding virtually identical Ct values. Cycling conditions were: 95°C for 10 min, followed by 40 cycles of 95°C/15 sec and 60°C/1 min. Product-specific amplification was ensured by melting curve analysis for each reaction. Relative transcript levels were calculated by normalization against the house-keeping gene encoding eukaryotic translation initiation factor 2-alpha kinase (*pk4*, PF3D7_0628200). All primer sequences are listed in Table S9.

Supplementary Text

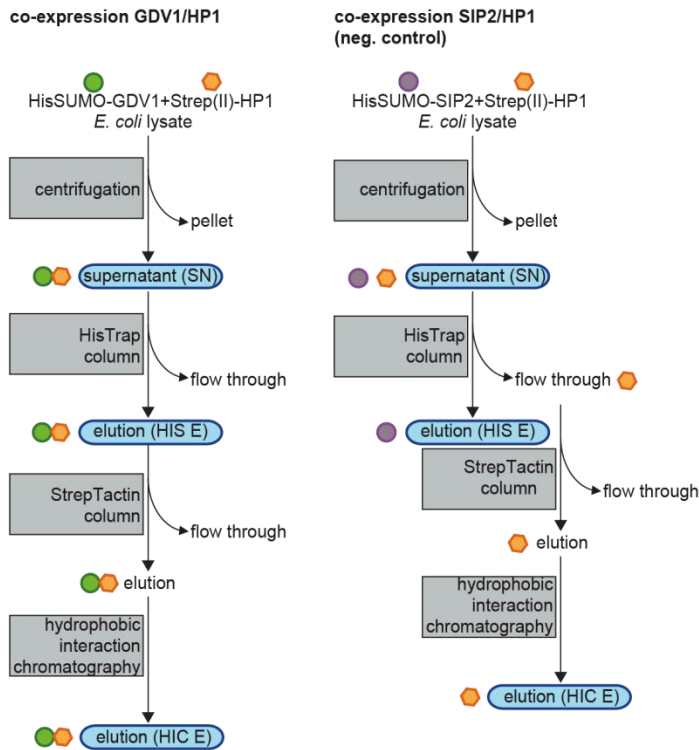
Deletion of the *gdv1* asRNA locus in F12 parasites resulted in a marked increase in *ap2-g* transcript levels (Fig. 4B, Fig. S6 and Table S8). Hence, to be able to knock-out the *gdv1* asRNA in 3D7 parasites we first had to modify the *ap2-g* locus such that AP2-G expression is prevented under default culture conditions. To achieve this in a most robust way we placed expression of AP2-G under control of two conditional expression systems. Using a single CRISPR/Cas9-based gene editing step we tagged AP2-G with a C-terminal GFP-DD tag and at the same time inserted a *glmS* riboswitch element into the 3' untranslated region (Fig. S8). The *glmS* riboswitch allows regulating gene expression at the level of the mRNA; in presence of the amino sugar glucosamine (GlcN) the *glmS* ribozyme structure mediates self-cleavage of the mRNA leading to its degradation (56-58). As expected, parasites did not express AP2-G-GFP-DD and failed to produce gametocytes when cultured in absence of Shield-1 and presence of GlcN. In presence of Shield-1 and absence of GlcN AP2-G-GFP-DD expression was detectable by IFA in the nuclei of some parasites and gametocytes were produced at a rate of 11.0% (+/- 0.3 SD) (Fig. S8).

Having established this conditional AP2-G loss-of-function mutant we next deleted the *gdv1* asRNA locus in these parasites (3D7/AP2-G-GFP-DD*glmS/gdv1*-asKO). 3D7/AP2-G-GFP-DD*glmS/gdv1*-asKO parasites still failed to produce gametocytes when AP2-G-GFP-DD expression was prevented in absence of Shield-1 and presence of GlcN. However, compared to the 3D7/AP2-G-GFP-DD*glmS* control line 3D7/AP2-G-GFP-DD*glmS/gdv1*-asKO parasites displayed a substantially increased sexual conversion rate of 39.3% (+/- 2.8 SD) when AP2-G-GFP-DD expression was stabilised, showing that the *gdv1*-asRNA antagonises the GDV1-dependent induction of gametocyte conversion.

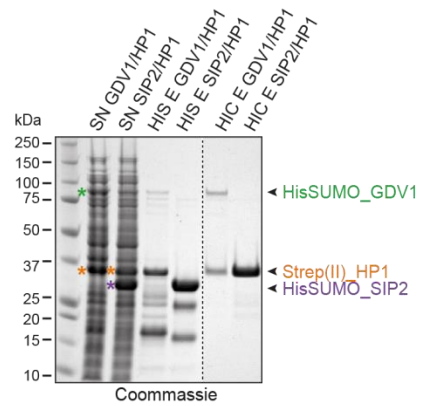
A



B



C



D

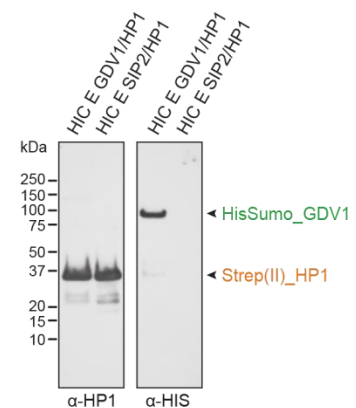


Fig. S1. GDV1 co-localises and interacts with HP1. (A) α -GFP (green) and α -HP1 (red) co-localisation IFAs in 3D7/GDV1-GFP-DD^{ON} trophozoites (T, 24-32 hpi), early schizonts (ES, 32-40 hpi) and late schizonts (LS, 40-48 hpi). Scale bar, 2.5 μ m. White frames refer to the magnified views in the rightmost images (scale bar, 0.5 μ m). DIC, differential interference contrast. Results are representative of three biological replicate experiments. (B) Flow chart of the purification approach used to demonstrate direct protein-protein interaction between GDV1 and HP1 co-expressed in *E.coli* as HisSumo-tagged GDV1 and Strep(II)-tagged HP1. Co-expression of a HisSUMO-tagged N-terminal fragment of the heterochromatin-associated ApiAP2 factor PfSIP2 (45) and Strep(II)-tagged HP1 was used as negative control. Samples highlighted in blue are shown in the Coomassie-stained polyacrylamide gel shown in panel C. (C) Coomassie-stained SDS-polyacrylamide gel. Lane 1: protein size standard. Lanes 2, 3: supernatants (SN) of bacterial lysates show co-expression of the respective fusion proteins GDV1/HP1 (lane 2) and SIP2/HP1 (lane 3) (asterisks). Lanes 4, 5: elution samples obtained after Ni²⁺ affinity purification (HIS E) of the GDV1/HP1 SN (lane 4) or the SIP2/HP1 SN (lane 5). Strep(II)-tagged HP1 co-purified specifically with HisSUMO-GDV1 (lane 4) but not with HisSUMO-SIP2 (lane 5). Lanes 6, 7: the Ni²⁺ column elution of the GDV1/HP1 sample (containing both HisSUMO-GDV1 and Strep(II)-HP1) and Ni²⁺ column flow through of the SIP2/HP1 negative control sample (containing Strep(II)-HP1) were further purified using StrepTactin affinity purification followed by hydrophobic interaction chromatography (HIC). Analysis of the HIC eluates (HIC E) show that HisSUMO-GDV1 co-purified with Strep(II)-HP1 (lane 6). (D) α -HP1 and α -HIS Western blot confirm the identities of HisSUMO-GDV1 and Strep(II)-HP1 in the HIC elution samples.

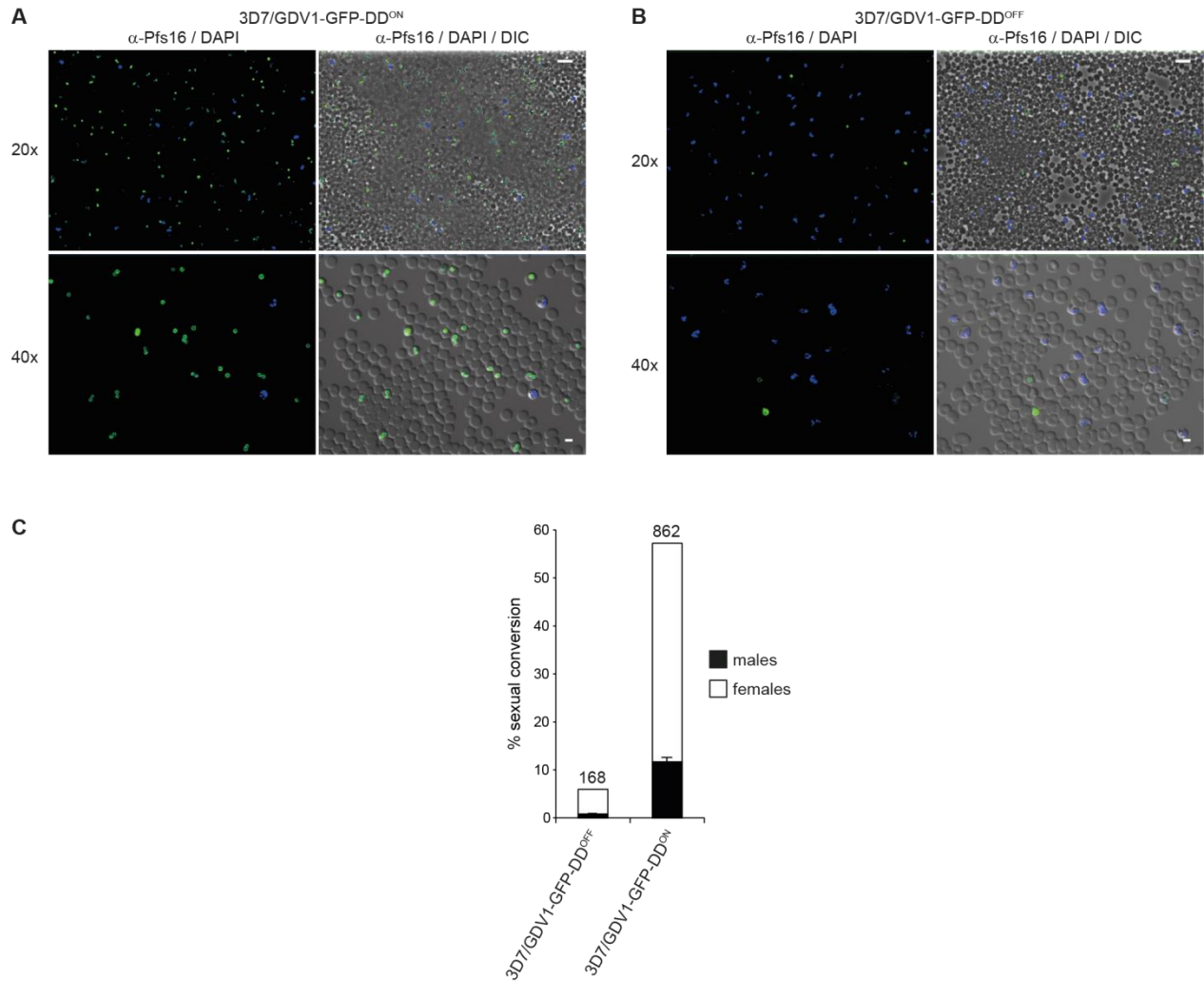


Fig. S2. GDV1 over-expression induces sexual commitment. (A,B) Overview images of IFAs performed on formaldehyde/glutaraldehyde-fixed cultures 38-46 hours after re-invasion (day 2) using α -Pfs16 antibodies, highlighting the large proportion of stage I gametocytes (green) in 3D7/GDV1-GFP-DD^{ON} (A) compared to 3D7/GDV1-GFP-DD^{OFF} (B) parasites. Nuclei were stained with DAPI. Scale bars, 15 μ m (20x magnification) and 5 μ m (40x magnification). (C) Proportion of male and female gametocytes in 3D7/GDV1-GFP-DD^{OFF} and 3D7/GDV1-GFP-DD^{ON} populations. Results represent the mean of three technical replicates (error bars represent SD). Total number of scored gametocytes is shown above the bars.

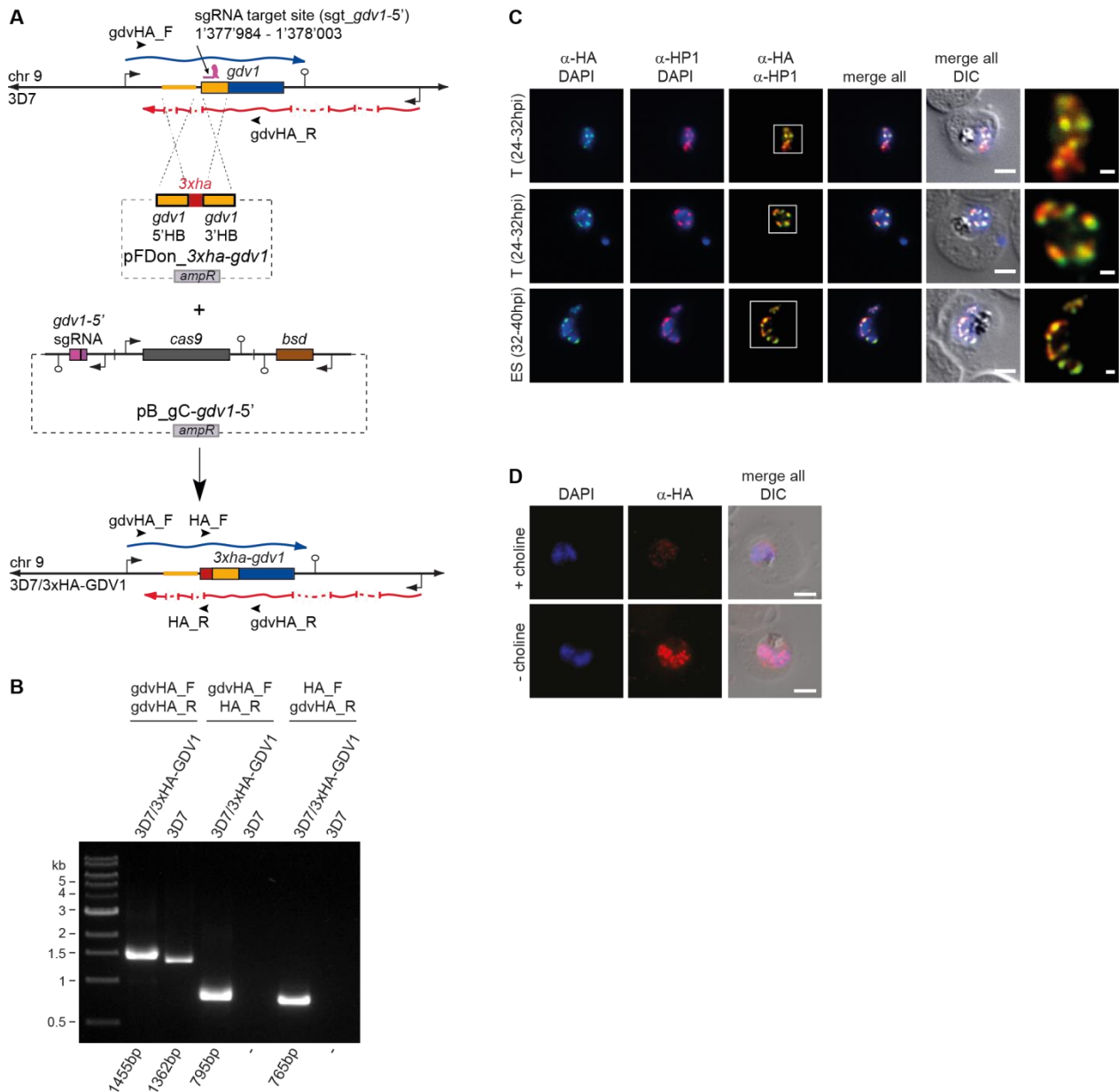


Fig. S3. Generation of the 3D7/3xHA-GDV1 line using CRISPR/Cas9 and expression of endogenous 3xHA-GDV1. (A) Schematic maps of the *gdv1* locus (PF3D7_0935400) in 3D7 parasites (top), the pFDon_3xha-gdv1 donor and pB_gC-gdv1-5' CRISPR/Cas9 transfection vectors (center), and the modified *gdv1* locus after CRISPR/Cas9-based genome editing in 3D7/3xHA-GDV1 parasites (bottom). The *gdv1* sense transcript and multi-exon antisense transcript (24) are indicated by undulated arrows in blue and red, respectively. The nucleotide positions of the *sgt_gdv1-5'* sgRNA target sequence is indicated (chromosome 9 coordinates). The pFDon_3xha-gdv1 donor plasmid contains a 3xha sequence (red) flanked on either side by a homology box (HB) (orange) for homology-directed repair. The pB_gC-gdv1-5' plasmid contains expression cassettes for SpCas9 (grey), the sgRNA (purple) and the *bsd* resistance marker (brown). Successful gene editing results in the expression of a N-terminally tagged 3xHA-GDV1. PCR primer binding sites used to confirm successful gene editing are indicated by

arrowheads. **(B)** PCR on gDNA from 3D7/3xHA-GDV1 and 3D7 wild-type parasites. Primers *gdvHA_F* and *gdvHA_R* bind to chromosomal sequences outside the HBs and amplify a 1455 bp or 1362 bp fragment from the edited or wild-type *gdv1* locus, respectively. The *gdvHA_F/HA_R* and *HA_F/gdvHA_R* primer combinations are specific for the edited locus and amplify 795 bp and 765 bp fragments, respectively. **(C)** α -HA (green) and α -HP1 (red) co-localisation IFAs in 3D7/3xHA-GDV1 trophozoites (T, 24-32 hpi) and early schizonts (ES, 32-40 hpi). Scale bar, 2.5 μ m. White frames refer to the magnified views in the rightmost images (scale bar, 0.5 μ m). DIC, differential interference contrast. Results are representative of two biological replicate experiments. **(D)** Representative α -HA (red) IFAs of 3D7/3xHA-GDV1 parasites cultured in presence or absence of 2 mM choline. Nuclei were stained with DAPI. Scale bar, 2.5 μ m. DIC, differential interference contrast.

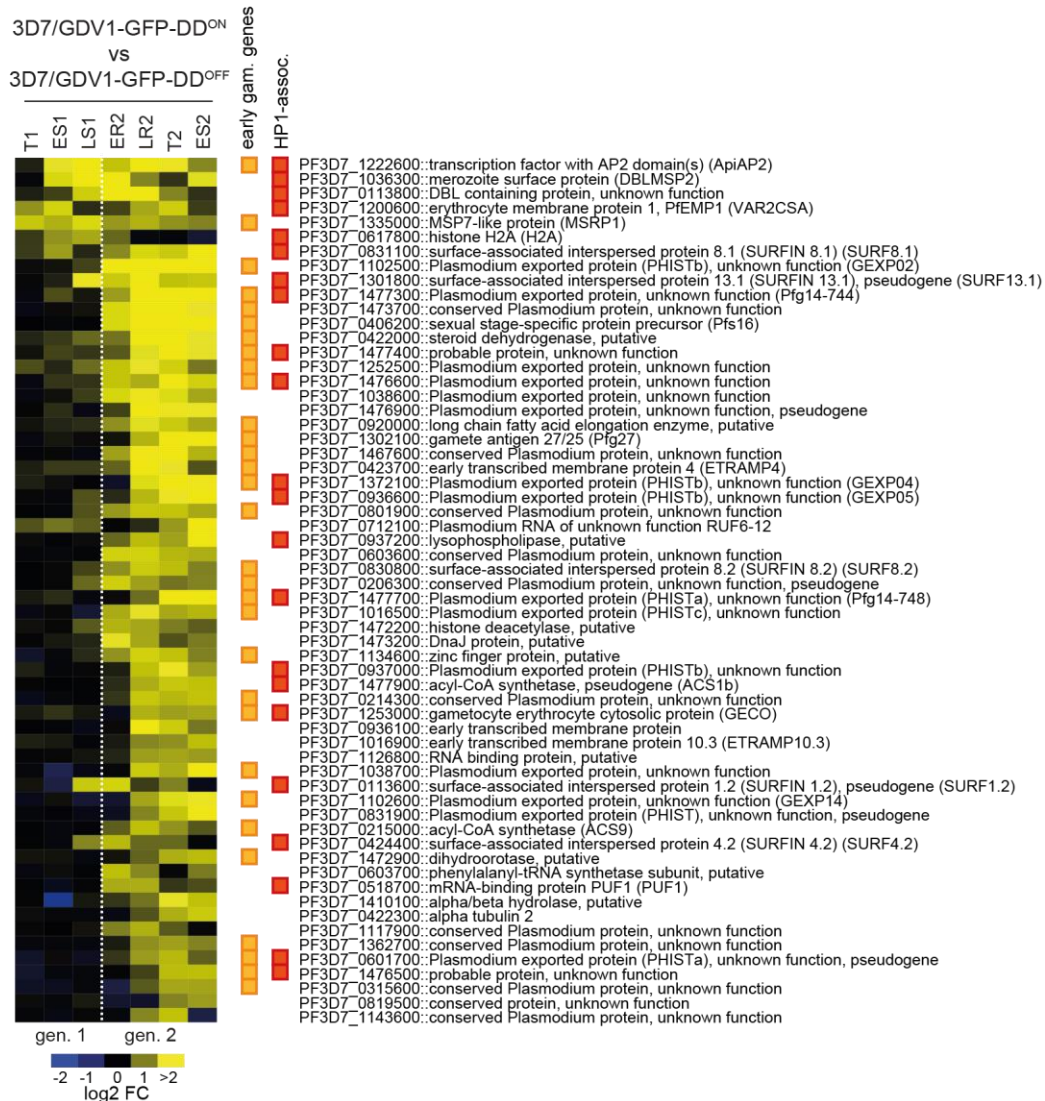


Fig. S4. Induction of GDV1-GFP-DD expression triggers a gametocyte-specific transcriptional response. The heatmap shows the temporal gene induction profiles of all genes with (1) higher transcript levels in 3D7/GDV1-GFP-DD^{ON} compared to the 3D7 reference pool (positive log₂ Cy5/Cy3 ratio), and (2) greater than 2-fold higher transcript levels in 3D7/GDV1-GFP-DD^{ON} vs 3D7/GDV1-GFP-DD^{OFF} (log₂ fold change >1) in any two of the seven consecutive TPs. HP1-associated genes identified previously (2) and in this study (Table S7) are highlighted by red boxes. Early gametocyte genes identified in previous studies (7, 8, 17) are highlighted by orange boxes. FC, fold change; gen., generation. T1/ES1/LS1, trophozoites, early schizonts, late schizonts in generation 1; ER2/LR2/T2/ES2, early ring stages, late ring stages, trophozoites, early schizonts in generation 2.

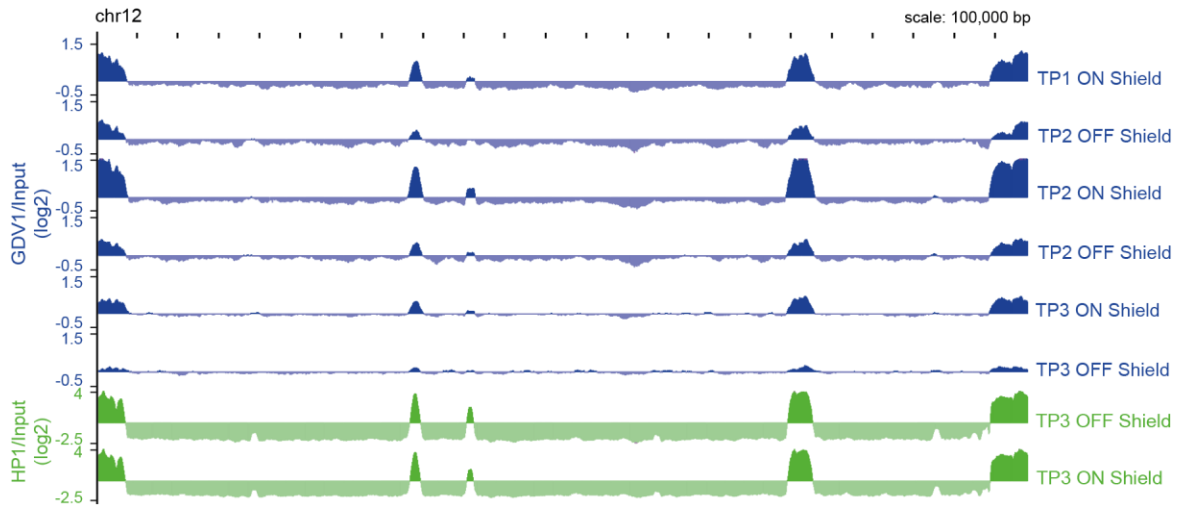


Fig. S5. Increased GDV1 occupancy at heterochromatic domains at all three TPs in 3D7/GDV1-GFP-DD^{ON} compared to 3D7/GDV1-GFP-DD^{OFF} parasites. ChIP-seq ratio tracks display relative enrichment (ChIP/input) of GDV1-GFP-DD (blue) or HP1 (green) along chromosome 12 in 3D7/GDV1-GFP-DD^{ON} parasites cultured in the presence of Shield-1 for two (TP1, 30-36 hpi), six (TP2, 34-40 hpi) or ten hours (TP3, 38-44 hpi) and in the matching control populations grown in the absence of Shield-1 (3D7/GDV1-GFP-DD^{OFF}).

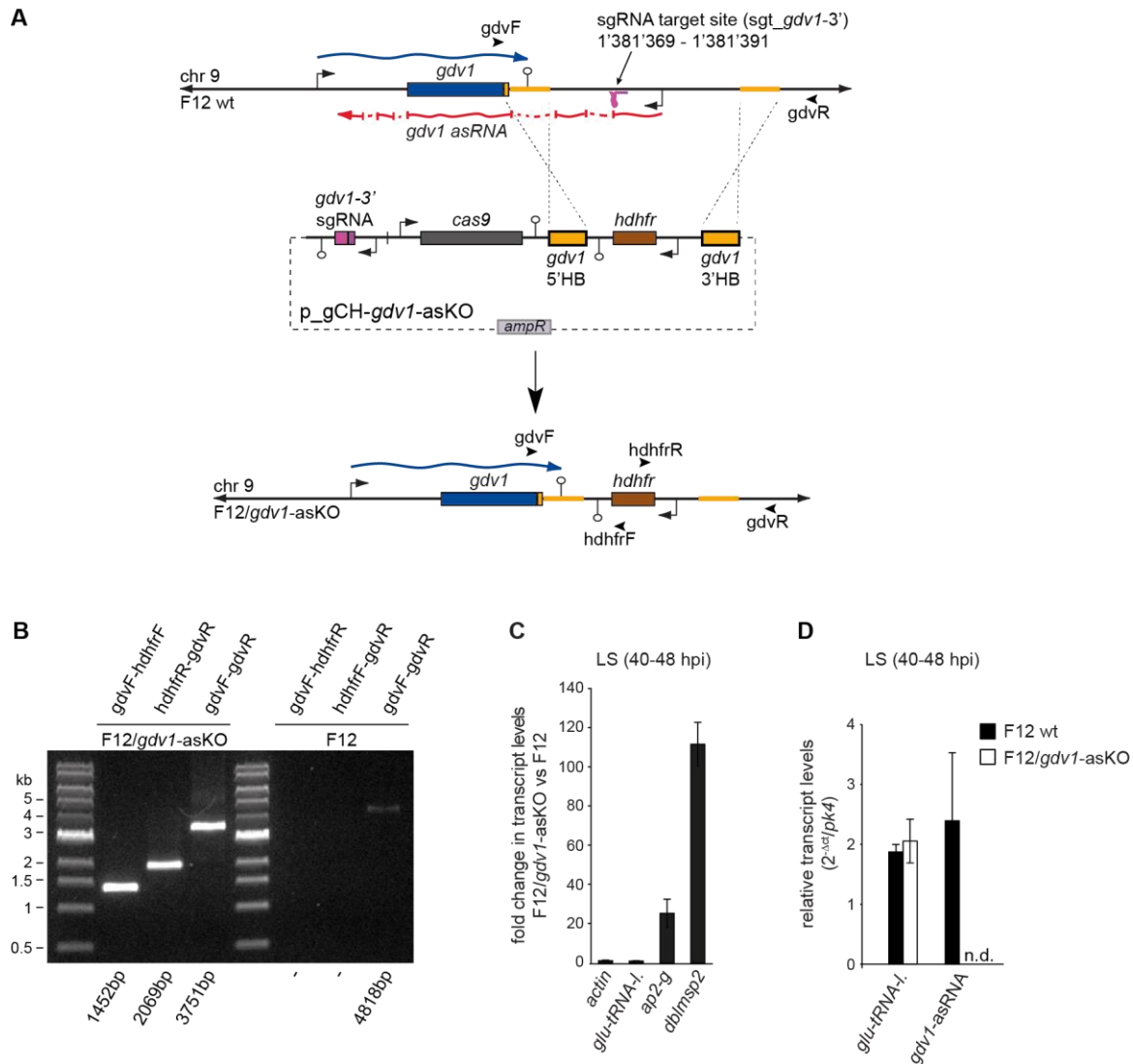


Fig. S6. Generation of the F12/*gdv1*-asKO parasite line using CRISPR/Cas9. (A) Schematic maps of the *gdv1* locus (PF3D7_0935400) in F12 parasites (top), the p_gCH-*gdv1*-asKO CRISPR/Cas9 transfection vector (center), and the modified *gdv1* locus after CRISPR/Cas9-based genome editing in F12/*gdv1*-asKO parasites (bottom). The *gdv1* sense transcript and multi-exon antisense transcript (24) are indicated by undulated arrows in blue and red, respectively. The nucleotide positions of the *sgt_gdv1-3'* sgRNA target sequence is indicated (chromosome 9 coordinates). The p_gCH-*gdv1*-asKO plasmid contains expression cassettes for SpCas9 (grey), the sgRNA (purple) and the *hdhfr* resistance marker (brown) flanked by two homology boxes (HB) (orange) for homology-directed repair. PCR primer binding sites used to confirm successful gene editing are indicated by arrowheads. (B) PCR on gDNA from F12/*gdv1*-asKO and F12 wild-type parasites. Primers *gdvF* and *gdvR* bind to chromosomal sequences outside the HBs and amplify a 3751 bp or 4818 bp fragment from the edited or wild-type *gdv1* locus, respectively. The *gdvF/hdhfrF* and *hdhfrR/gdvR* primer combinations are specific for the edited locus and amplify 1452 bp and 2069 bp fragments, respectively. (C) RT-qPCR data confirming the increase in *ap2-g* and *dblmsp2* transcript levels in F12/*gdv1*-asKO compared to F12 wild-type parasites (results are the mean of three biological replicates; error bars represent SD). *actin*

(PF3D7_1264200)/*glu-tRNA-l*.(PF3D7_1331700), control genes. **(D)**, RT-qPCR showing the absence of *gdl* asRNA in F12/*gdl*-asKO parasites. Values represent expression levels relative to the house-keeping gene encoding eukaryotic translation initiation factor 2-alpha kinase (*pk4*, PF3D7_0628200). *glu-tRNA-l*. (PF3D7_1331700), control gene. Results are the mean of three biological replicates (error bars represent SD). n.d., not detectable.

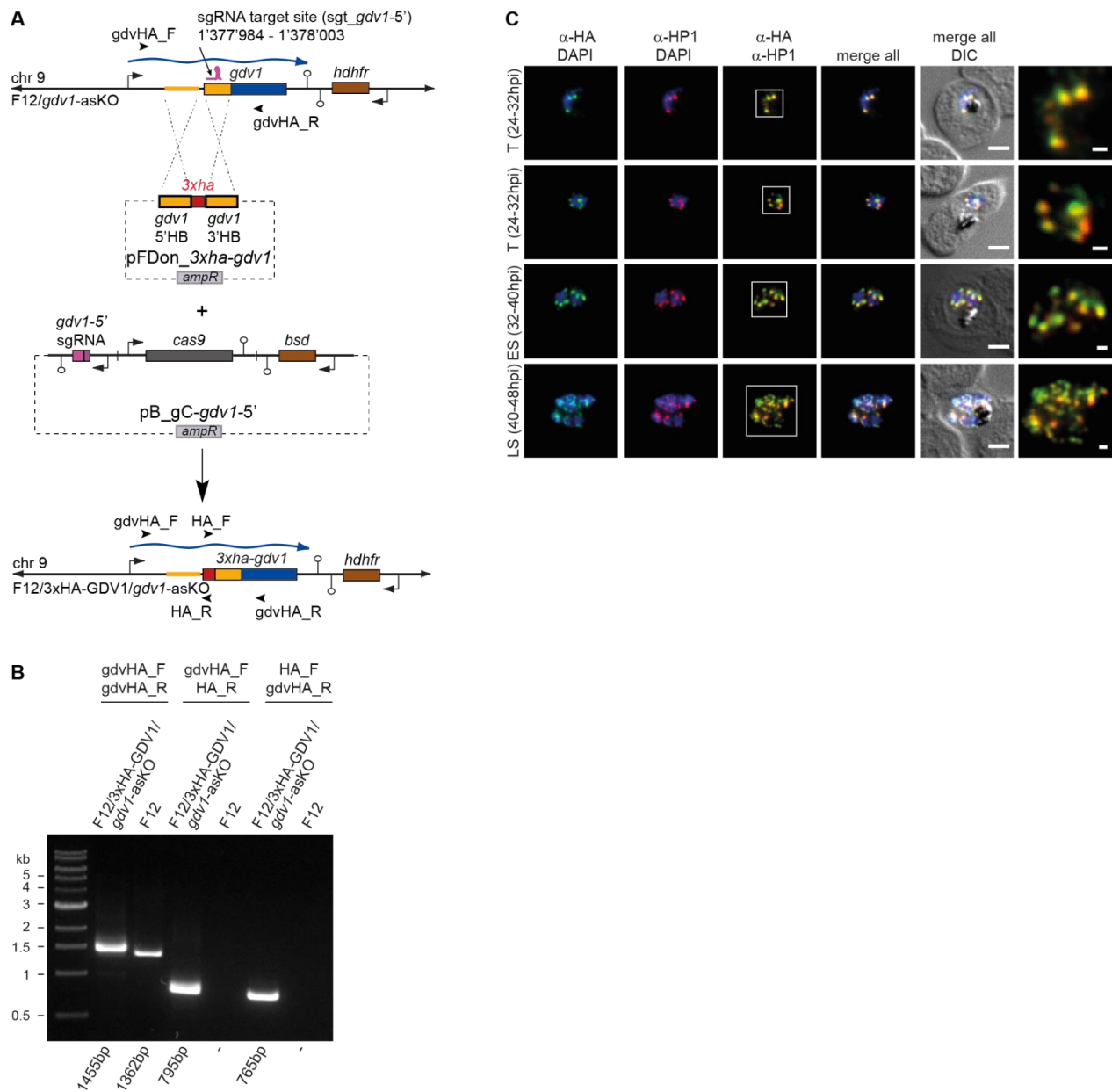


Fig. S7. Generation of the F12/3xHA-GDV1/*gdv1*-asKO line using CRISPR/Cas9 and expression of endogenous 3xHA-GDV1. (A) Schematic maps of the *gdv1* locus (PF3D7_0935400) in F12/*gdv1*-asKO parasites (top), the pFDon_3xha-*gdv1* donor and pB_gC-*gdv1*-5' CRISPR/Cas9 transfection vectors (center), and the modified *gdv1* locus after CRISPR/Cas9-based genome editing in F12/3xHA-GDV1/*gdv1*-asKO parasites (bottom). The *gdv1* sense transcript is indicated by an undulated arrow in blue. The nucleotide positions of the *sgt_gdv1*-5' sgRNA target sequence is indicated (chromosome 9 coordinates). The pFDon_3xha-*gdv1* donor plasmid contains a *3xha* sequence (red) flanked on either side by a homology box (HB) (orange) for homology-directed repair. The pB_gC-*gdv1*-5' plasmid contains expression cassettes for SpCas9 (grey), the sgRNA (purple) and the *bsd* resistance marker (brown). Successful gene editing results in the expression of a N-terminally tagged 3xHA-GDV1. PCR primer binding sites used to confirm successful gene editing are indicated by arrowheads. (B)

PCR on gDNA from F12/3xHA-GDV1/*gdv1*-asKO and F12 wild-type parasites. Primers *gdvHA_F* and *gdvHA_R* bind to chromosomal sequences outside the HBs and amplify a 1455 bp or 1362 bp fragment from the edited or wild-type *gdv1* locus, respectively. The *gdvHA_F/HA_R* and *HA_F/gdvHA_R* primer combinations are specific for the edited locus and amplify 795 bp and 765 bp fragments, respectively. (C) α -HA (green) and α -HP1 (red) co-localisation IFAs in F12/3xHA-GDV1/*gdv1*-asKO trophozoites (T, 24-32 hpi), early schizonts (ES, 32-40 hpi) and late schizonts (LS, 40-48 hpi). Scale bar, 2.5 μ m. White frames refer to the magnified views in the rightmost images (scale bar, 0.5 μ m). DIC, differential interference contrast. Results are representative of two biological replicate experiments.

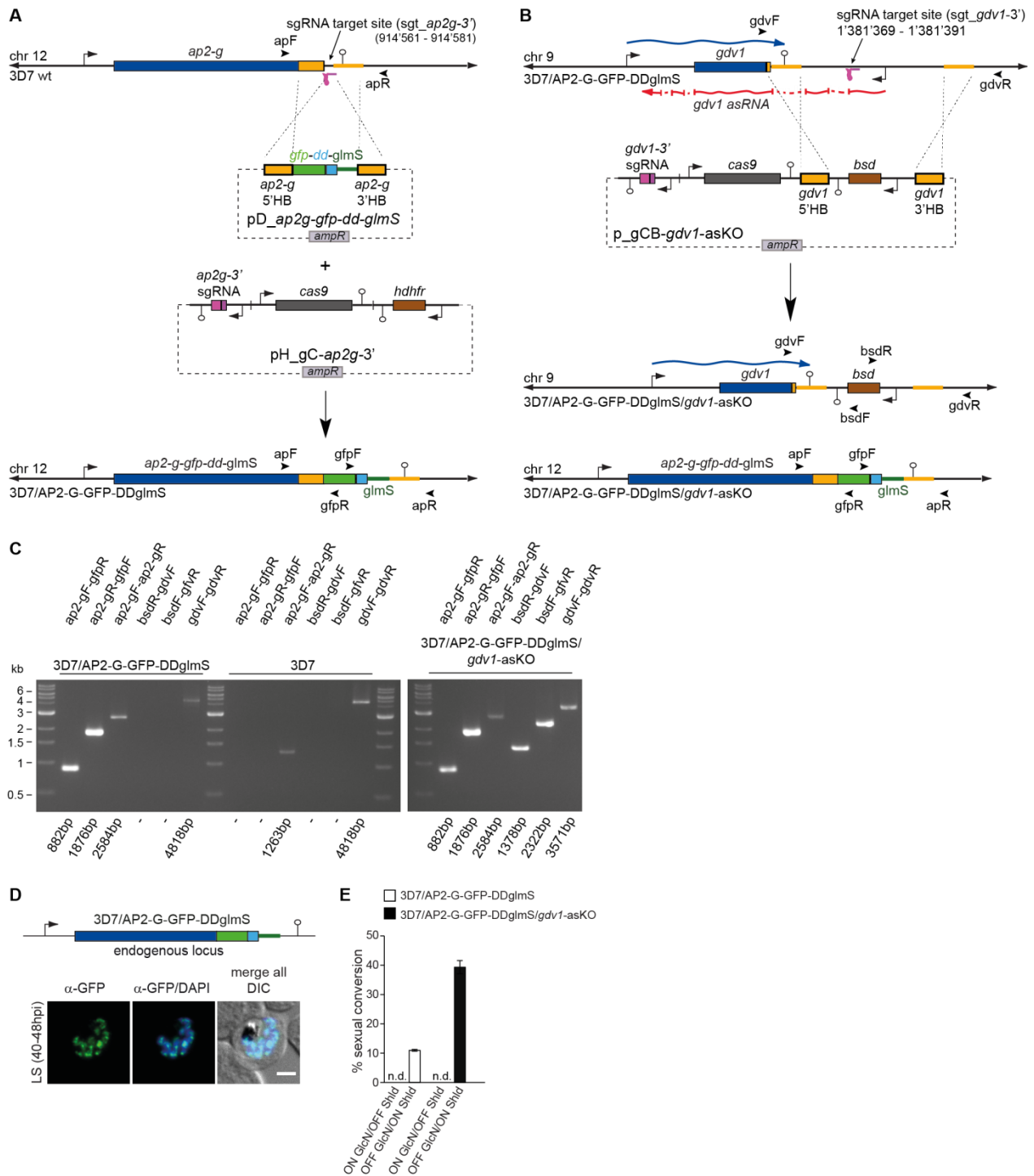


Fig. S8. Generation of the 3D7/AP2-G-GFP-DDglmS and 3D7/AP2-G-GFP-DDglmS/*gdv1*-askO parasite lines using CRISPR/Cas9. (A) Schematic maps of the *ap2-g* locus (PF3D7_1222600) in 3D7 parasites (top), the pD_ *ap2-g-gfp-dd-glmS* donor and pH_gC-*ap2g-3'* CRISPR/Cas9 transfection vectors (center), and the modified *ap2-g* locus after CRISPR/Cas9-based genome editing in 3D7/AP2-G-GFP-DDglmS parasites (bottom). The nucleotide positions of the *sgt_ap2g-3'* sgRNA target sequence is indicated (chromosome 12 coordinates). The

pD_ *ap2-g-gfp-dd-glmS* donor plasmid contains a *gfp-dd-glmS* fusion sequence flanked on either side by a homology box (HB) (orange) for homology-directed repair. The pH_gC-*ap2g-3'* plasmid contains expression cassettes for SpCas9 (grey), the sgRNA (purple) and the *hdhfr* resistance marker (brown). Successful gene editing results in the expression of a C-terminally tagged AP2-G-GFP-DD fusion protein that is under control of the *glmS* riboswitch system (56). PCR primer binding sites used to confirm successful gene editing are indicated by arrowheads. **(B)** Schematic maps of the *gdv1* locus (PF3D7_0935400) in 3D7/AP2-G-GFP-DDglmS parasites (top), the p_gCB-*gdv1*-asKO CRISPR/Cas9 transfection vector (center), and the modified *gdv1* and *ap2-g* loci after CRISPR/Cas9-based genome editing in 3D7/AP2-G-GFP-DDglmS/*gdv1*-asKO parasites (bottom). The *gdv1* sense transcript and multi-exon antisense transcript (24) are indicated by undulated arrows in blue and red, respectively. The nucleotide positions of the *sgt_gdv1-3'* sgRNA target sequence is indicated (chromosome 9 coordinates). The p_gCB-*gdv1*-asKO plasmid contains expression cassettes for SpCas9 (grey), the sgRNA (purple) and the *bsd* resistance marker (brown) flanked by two homology boxes (HB) (orange) for homology-directed repair. PCR primer binding sites used to confirm successful gene editing are indicated by arrowheads. **(C)** PCR on gDNA from 3D7/AP2-G-GFP-DDglmS/*gdv1*-asKO, 3D7/AP2-G-GFP-DDglmS and 3D7 wild-type parasites. Primers apF and apR bind to chromosomal sequences outside the *ap2-g* HBs and amplify a 2584 bp or 1263 bp fragment from the edited or wild-type *ap2-g* locus, respectively. Primers *gdvF* and *gdvR* bind to chromosomal sequences outside the *gdv1* HBs and amplify a 3751 bp or 4818 bp fragment from the edited or wild-type *gdv1* locus, respectively. The apF/*gfpR* and apR/*gfpF* primer combinations are specific for the edited *ap2-g* locus and amplify 882 bp and 1876 bp fragments, respectively. The *bsdR/gdvF* and *bsdF/gdvR* primer combinations are specific for the edited *gdv1* locus and amplify 1378 bp and 2322 bp fragments, respectively. **(D)** Endogenous *ap2-g* locus in the 3D7/AP2-G-GFP-DDglmS line and α -GFP IFA showing AP2-G-GFP-DD expression in a late schizont (LS, 40-48 hpi) from a 3D7/AP2-G-GFP-DDglmS culture grown in presence of Shield-1 and absence of glucosamine (GlcN). DIC, differential interference contrast. Scale bar, 2.5 μ m. Results are representative of three biological replicates. **(E)** Sexual conversion rates in 3D7/AP2-G-GFP-DDglmS and 3D7/AP2-G-GFP-DDglmS/*gdv1*-asKO parasites cultured either in presence of GlcN/absence of Shield-1 (AP2-G-GFP-DD expression prevented) or absence of GlcN/presence of Shield-1 (AP2-G-GFP-DD expression permitted) (results are the mean of three biological replicates (>200 infected RBCs counted per sample); error bars indicate SD).

Table S1. Potential HP1-interacting proteins identified by LC-MS/MS in the eluates of three independent Co-IP experiments. Gene IDs and annotations have been retrieved from PlasmoDB (www.plasmodb.org). This table lists all proteins detected in all three HP1-GFP Co-IP eluates (Co-IP Exp#1-3) and undetected in all negative control eluates. Note that for each experiment the sequence coverage and number of unique peptides indicated derive from either the 2 M arginine or subsequent 2% SDS elution samples, whichever displayed the higher number of unique tryptic peptides detected (see also Table S3). Cov, % sequence coverage; Pep, number of unique tryptic peptides detected.

GeneID	Description	Co-IP Exp#1		Co-IP Exp#2		Co-IP Exp#3	
		Cov	Pep	Cov	Pep	Cov	Pep
PF3D7_1220900	heterochromatin protein 1 (HP1)	77.82	30	65.79	23	71.43	24
PF3D7_0935400	gametocyte development protein 1 (GDV1)	43.91	19	9.68	6	22.20	10
PF3D7_0818200	14-3-3 protein (14-3-3I)	43.89	7	17.94	3	10.31	3
PF3D7_1451200	conserved Plasmodium protein, unknown function	17.42	24	14.10	14	15.43	21
PF3D7_1441400	FACT complex subunit SSRP1, putative (FACT-S)	11.46	5	9.49	4	7.91	3
PF3D7_0517400	FACT complex subunit SPT16, putative (FACT-L)	1.14	1	8.41	8	3.24	3
PF3D7_1023900	chromodomain-helicase-DNA-binding protein 1 homolog, putative (CHD1)	0.45	1	0.45	1	5.26	12
PF3D7_1357400	conserved Plasmodium protein, unknown function	1.70	2	3.56	3	3.48	3
PF3D7_1456000	transcription factor with AP2 domain(s) (ApiAP2)	2.91	4	0.80	1	3.20	3

Table S2. Potential GDV1-interacting proteins identified by LC-MS/MS in the eluates of three independent Co-IP experiments. Gene IDs and annotations have been retrieved from PlasmoDB (www.plasmodb.org). This table lists all proteins detected in all three GDV1-GFP-DD Co-IP eluates (Co-IP Exp#1-3) and undetected in all negative control eluates (see also Table S4). Cov, % sequence coverage; Pep, number of unique tryptic peptides detected.

GeneID	Description	Co-IP Exp#1		Co-IP Exp#2		Co-IP Exp#3	
		Cov	Pep	Cov	Pep	Cov	Pep
PF3D7_0505800	small ubiquitin-related modifier, putative (SUMO)	54	5	46	4	37	2
PF3D7_1220900	heterochromatin protein 1 (HP1)	50.38	14	28.95	9	23.31	6
PF3D7_0935400	gametocyte development protein 1 (GDV1)	32.89	19	23.54	10	18.36	9
PF3D7_1211800	polyubiquitin (PfpUB)	44.62	1	21	1	21	1
PF3D7_1451200	conserved Plasmodium protein, unknown function	15.82	24	20.81	29	5.72	7
PF3D7_1023900	chromodomain-helicase-DNA-binding protein 1 homolog, putative (CHD1)	10.16	30	8.74	23	5.44	13
PF3D7_1027800	60S ribosomal protein L3, putative	3.11	1	3.11	1	3.11	1
PF3D7_1447000	40S ribosomal protein S2, putative	2.94	1	3.31	1	3.31	1

Table S3. Mass spectrometry results of the HP1-GFP co-IP experiments. This file lists all proteins and peptides identified by Mascot and Sequest HT searches of the results obtained from LC-MS/MS analysis of protein elutions 1 (E1_Arg) and 2 (E2_SDS) obtained after HP1-GFP co-IP (HP1 Co-IP) or negative control IPs (neg. control). The experiments have been performed in three biological replicates (#1-3). The file contains 12 worksheets. (xlsx format).

Table S4. Mass spectrometry results of the GDV1-GFP-DD co-IP experiments. This file lists all proteins and peptides identified by Mascot and Sequest HT searches of the results obtained from LC-MS/MS analysis of protein elutions (E_SDS) obtained after GDV1-GFP co-IP (GDV1 Co-IP) or negative control IPs (neg. control). The experiments have been performed in three biological replicates (#1-3). The file contains 6 worksheets. (xlsx format).

Table S5. Processed microarray data obtained from 3D7/GDV1-GFP-DD parasites. Columns A-B: Gene ID and gene annotation. Column C: HP1 target genes previously identified by ChIP-on-chip (2) and in this study (Table S7). Column D: known early gametocyte markers (7, 8, 17). Columns E-K: Cy5/Cy3 log₂ ratios for all transcripts and seven TPs harvested from 3D7/GDV1-GFP-DD^{OFF} parasites. Columns L-R: Cy5/Cy3 log₂ ratios for all transcripts and seven TPs harvested from 3D7/GDV1-GFP-DD^{ON} parasites. Column S-Y: fold change in gene expression (log₂) in 3D7/GDV1-GFP-DD^{ON} compared to 3D7/GDV1-GFP-DD^{OFF} parasites for each of the seven paired TPs. Column Z: mean fold change in gene expression in 3D7/GDV1-GFP-DD^{ON} compared to 3D7/GDV1-GFP-DD^{OFF} parasites across all seven TPs. Column AA: SAM significance q-values (% fdr). Column AB: significantly up-regulated (u) or down-regulated (d) genes. T1/ES1/LS1, trophozoites, early schizonts, late schizonts in generation 1; ER2/LR2/T2/ES2, early ring stages, late ring stages, trophozoites, early schizonts in generation 2. (xlsx format).

Table S6. Processed microarray data obtained with F12/GDV1-GFP-DD parasites. Columns A-B: Gene ID and gene annotation. Column C: HP1 target genes previously identified by ChIP-on-chip (2) and in this study (Table S7). Column D: known early gametocyte markers (7, 8, 17). Columns E-K: Cy5/Cy3 log₂ ratios for all transcripts and seven TPs harvested from F12/GDV1-GFP-DD^{OFF} parasites. Columns L-R: Cy5/Cy3 log₂ ratios for all transcripts and seven TPs harvested from F12/GDV1-GFP-DD^{ON} parasites. Column S-Y: fold change in gene expression (log₂) in F12/GDV1-GFP-DD^{ON} compared to F12/GDV1-GFP-DD^{OFF} parasites for each of the seven paired TPs. Column Z: mean fold change in gene expression in F12/GDV1-GFP-DD^{ON} compared to F12/GDV1-GFP-DD^{OFF} parasites across all seven TPs. Column AA: SAM significance q-values (% fdr). Column AB: significantly up-regulated (u) or down-regulated (d) genes. T1/ES1/LS1, trophozoites, early schizonts, late schizonts in generation 1; ER2/LR2/T2/ES2, early ring stages, late ring stages, trophozoites, early schizonts in generation 2. (xlsx format).

Table S7. GDV1-GFP-DD and HP1 ChIP-seq enrichment values. ChIP/input enrichment values were calculated over each coding region of the Pf_3D7_v3 reference genome in 3D7/GDV1-GFP-DD^{ON} and 3D7/GDV1-GFP-DD^{OFF} parasites at TPs 1-3 (30-36 hpi, 34-40 hpi, 38-44 hpi). Columns A-B: Gene ID and gene annotation. Column C: chromosome number. Columns D-E: Nucleotide positions at the start and end of each gene. Column F: HP1-associated genes (HP1 ChIP/input >1 in 3D7/GDV1-GFP-DD^{OFF} control parasites at TP3). Column G: known early gametocyte markers (7, 8, 17). Columns H-M: GDV1-GFP-DD ChIP/input values

for each population and TP. Columns N-P: fold change in GDV1-GFP-DD occupancy between parasites cultured in the presence or absence of Shield-1 for each TP. Columns Q-R: HP1 ChIP/input values for both populations at TP3. Column S: log₂ fold change in HP1 occupancy between parasites cultured in the presence or absence of Shield-1 for TP3. (xlsx format).

Table S8. Processed RNA-seq data of sense transcripts obtained from F12 wild-type and F12/*gdv1*-asKO parasites. Columns A-B: Gene ID and gene annotations. Column C: HP1 target genes previously identified by ChIP-on-chip (2) and in this study (Table S7). Columns D-E: RPKM values for early schizonts (32-40 hpi) of F12 wild-type and F12/*gdv1*-asKO parasites. Column F: fold change (FC) in transcript abundance in F12/*gdv1*-asKO compared to F12 wild-type early schizonts (32-40 hpi). Columns G-H: RPKM values for late schizonts (40-48 hpi) of F12 wild-type and F12/*gdv1*-asKO parasites. Column I: fold change (FC) in transcript abundance in F12/*gdv1*-asKO compared to F12 wild-type late schizonts (40-48 hpi). Column J: Genes consistently up-regulated (up) or down-regulated (down) in both time points in F12/*gdv1*-asKO compared to F12 wild-type parasites. Genes with RPKM values < 3 in both samples per time point are highlighted in grey and were excluded from downstream analyses. (xlsx format)

Table S9. Oligonucleotides used in this study.